UNIVERSITY OF CALIFORNIA
RIVERSIDE

Kinetics of Pyrrhotite Oxidation in Seawater: Implications for Mining Seafloor Hotsprings

A Thesis submitted in partial satisfaction
of requirements for the degree of

Masters of Science

in

Geological Sciences

by

Gina Yolanda Romano

December 2012

Thesis Committee:

Dr. Michael McKibben, Chairperson

Dr. Timothy Lyons

Dr. Gordon Love

The Thesis of Gina Yolanda Romano is approved:

_____

_____

_____

Committee Chairperson

University of California, Riverside

Acknowledgements

I graciously acknowledge my committee members, especially Mike: thank you for always giving me more to think about, and for letting me be a part of this project, which I have become enormously passionate about. I am lucky to be able to directly apply this research to my exiting new career in industry.

Thank you to Laura Bilenker for many helpful conversations and even more helpful laughs. It was a great honor to do this project with you.

Thank you to the Lyons lab for the use of and assistance with the ICP-MS, especially Jeremy Owens. I am indebted to for your endless patience. Also thank you to Krassimir Bohzilov and CFAMM for the use of the SEM.

To my family: thank you for your endless support. I owe all my successes to you. Most of all I want to thank my Mom. You always push me to go after my dreams, never to give up, and are cheering me on the whole way. I wouldn't be where I am today without you.

Table of Contents

List of Figures

ABSTRACT

Laboratory experiments have been performed to evaluate the effects of pH, temperature, dissolved oxygen, and mineral surface area on the rate of oxidation of pyrrhotite in seawater. Experiments employed to determine these effects utilized temperature-controlled circulation baths, Teflon reaction vessels, synthetic seawater, and pure, hand-sorted natural pyrrhotite crystals. Both batch and flow-through reactor methods were used and reaction products were analyzed using inductively coupled plasma-mass spectrometry (ICP-MS). The rate law takes the following form:

$$R_{sp\ (Fe(1-x)S)} = -k\ (M_{H+})^{a}(M_{O2(aq)})^{b} \qquad \text{Eq. 1}$$

where R is the specific oxidation rate of pyrrhotite (moles/m^2 sec), k is the rate constant (a function of temperature and surface area), and a and b are reaction orders for reactant concentrations (M), determined experimentally. The isolation method was used to obtain the reaction order of each reactant on the basis of initial rates. The rate law for the oxidation of pyrrhotite in seawater derived in this study is:

$$R_{sp(Fe(1-x)S)} = -5.38 \times 10^{-8}\ (M_{H+})^{0.08\pm0.03}\ (M_{O2(aq)})^{0.30\pm0.07} \qquad \text{Eq. 2}$$

The value for k is averaged from runs at 22.0^{o}C, which was used at the primary run temperature for convenience. Values for k from all runs are in Appendix A.

Data from batch reactor experiments indicated positive influences of oxidant concentration, surface area, temperature, and [H^+] on the initial rate. Pyrrhotite oxidizes significantly faster than chalcopyrite, providing an upper limit to the anthropogenic and natural inorganic weathering rates of seafloor massive sulfide (SMS) deposits. Inorganic rates are most

relevant to rapid seafloor mining timespans (minutes to days), within which significant bacterial colonization of freshly ground sulfide mineral surfaces is not likely to occur (e.g., McBeth *et al*., 2011). In the future, microbial studies will be needed in order to quantify the catalyzing or inhibitory effects of bacteria on natural, in situ seafloor pyrrhotite oxidation using this study as a baseline.

1. INTRODUCTION

The United Nations Department of Economic and Social Affairs (DESA) has predicted that the global population will rise above 10 billion by 2100 (Heilig *et al*., 2012). It is not impossible to support a population that size, however it will require significantly more resources and many valuable commodities are already near depletion. The oceans are a largely untapped resource for economic minerals that contain base, ferro-alloy and precious metals. A rapid increase in the price of transition metals in recent years has piqued interest in deep sea *in situ* mining of seafloor massive sulfide (SMS) deposits (Hoagland *et al*., 2010).

Sulfide-rich hydrothermal vents known as “black smokers” were first discovered in 1979 on the East Pacific Rise at 21^{o}N through a joint French-American submersible investigation (Spiess *et al*., 1980). This has become the type locality for high temperature hydrothermal vents. More vents have since been discovered around the globe at a variety of tectonic settings including mid ocean ridges (MORs), back arc rift basins, and transform fracture zones (German, *et al*., 1993; German *et al*., 1995).

Within these tectonically active zones, seawater can penetrate deeply along fractures in oceanic crust (2-4 km) and become heated by magma and young hot rock. The geothermally heated water (≤360^{o}C) dissolves elements (i.e. S, Cu, Mn, Co, Ni) from seafloor crust. Some dissolved sulfide is produced by thermochemical reduction of the sulfate in seawater. The pregnant solution is convected upward through cracks and fissures in basalt and emerges on the ocean floors (Mills, 1995; Von Damm, 1990). Chimney growth is initiated when geothermally-heated waters are rapidly quenched by ambient seawater, which causes insoluble phases to precipitate (Fornari & Embly, 1995). Over time chimneys can grow to up to 15 m in height and along with surrounding sulfide mounds and debris, are known as seafloor massive sulfide (SMS) deposits.

While the concentration of sulfide minerals in SMS deposits varies at each locality, the most common constituents are Fe, Zn, Cu and Pb sulfides. Fe, Zn, and Cu sulfides are the first to precipitate from vents, almost instantaneously when hot, acidic, reducing fluids mix with seawater (Mottl & McConachy, 1990). Immediately after the precipitation of metal sulfides, Fe oxides precipitate and continue to rise in the buoyant plume (Rudwick & Enfield, 1993). Three types of neutrally-buoyant plume composition are observed: 1) Fe as the predominant element in sulfide and oxide phases, 2) rare earth elements scavenged from seawater onto Fe oxide surfaces, and 3) Cu and Zn preferentially partitioned into sulfide phases (Mills, 1995).

Massive sulfide deposits have been cored in several localities across MORs. The facies differ from locality to locality, but most stratigraphic sections follow a pattern of basalt overlain by turbidites, sediment with sulfide veins and impregnation, sulfide vein sediment, massive to semi-massive sulfides, and clastic sulfides, decreasing with depth (Duckworth, 1998). In the

northeast Pacific Ocean, pyrrhotite was found to be the dominant sulfide facies in Legs 139 and 169 of the Ocean Drilling Program (ODP), followed by pyrite, magnetite, sphalerite, and chalcopyrite in decreasing concentrations (Davis *et al*., 1992; Duckworth *et al*., 1994). With the little information available with regards to the geochemistry of the vents, there is even less known of the geochemistry of pyrrhotite precipitation and dissolution in seawater.

The interest in mining SMS deposits will be enacted this year when Nautilus Minerals, Inc. go into production at the world's first deep sea copper-gold mine, Solwara 1, in the Bismarck Sea (Loudon, 2011). Nautilus currently holds nearly 600,000 square km of tenement licenses and exploration permits in the territorial waters of Papua New Guinea, Fiji, Tonga, Solomon Islands, and New Zealand, with future plans to tap rift and back arc basin SMS deposits in the Pacific and Atlantic. The publically-held Nautilus is not alone; there are also private companies in Australia, Russia, China and elsewhere who also hold deep-sea exploration tenements. SMS mining would not have been profitable a decade ago, but with the demand for copper and gold prices rising over five times what it was ten years ago, the race is on to mine the seafloor.

There are unique incentives to seafloor mining that make it more attractive than traditional land mining of sulfides, including higher ore grades, smaller mine area footprint, little overburden, and conveniently available technology; but these are accompanied by important yet unanswered questions about the potential environmental effects, including localized sulfuric acid generation. Currently there is a paucity of data on the oxidation kinetics of sulfide minerals i.e. chalcopyrite, pyrite, pyrrhotite, galena, and sphalerite, in seawater. Specifically, pyrrhotite is an interesting sulfide mineral because it is a major non-economic component of SMS deposits

that will be disposed of on or above the seafloor during mining (Gwyther, 2008). Pyrrhotite oxidizes rapidly *via* an irreversible, acid-producing reaction, which could result in acid mine drainage (Belzile, 2004; Janzen, 1998; Pratt, 1994).

Acid mine drainage can occur when sulfides are exposed to oxygenated surface waters during mining of terrestrial deposits (i.e. coals or metal ores). Sulfide minerals oxidize when in the presence of oxygen and water, which releases sulfur oxyanions and protons. Sulfuric acid, produced as a by-product from sulfide oxidation, is hazardous to plant and animal life, and can be found in concentrations ranging from 100 - 50,000 ppm in mine waste waters (Hoffert, 1947; Johnson, 2003,). Sulfuric acid produced from sulfide oxidation is capable of further solubilizing various elements, including detrimental heavy metals (e.g. Blodau, 2006) and these can be leached or mobilized into water. Although contaminated water can sometimes be contained and treated, its release can cause catastrophic and environmentally-damaging events - e.g. Wheal Jane mine, UK 1992 or Aznalcollar – Los Frailes, Spain 1998 (Johnson & Hallberg, 2005; Simón *at al*., 1999).

A deep sea SMS mine has the potential to produce similar effects to acid mine drainage. This may occur locally on the seafloor where mining activities are taking place, near the sea surface during on-ship processing of ore, and potentially again, during the deep disposal of fine mining effluents near the sea floor. Conditions near the sea floor are very different from continental mining settings; there is less oxygen, temperatures are colder (away from vents), and a higher natural pH due to the buffering capacity of seawater, which means the results of SMS mining cannot be predicted by extension of terrestrial studies. In addition to the natural weathering processes that occur constantly on the seafloors, anthropogenic processes will

pulverize and expose the SMS to higher temperatures and concentrations of oxygen as the ore is slurried to surface ships for processing. On-board processing will decrease grain sizes, which will increase the grain surface areas and increase reactivity by creating more, fresh sulfide surfaces. Therefore, the waste effluent, pumped back to near the sea floor, will consist of sulfide fines that will be highly reactive.

The significance and extent of these effects are currently unknown. Any local change in pH due to mining could affect seafloor ecology, analogous to groundwater contamination by acid mine drainage or widespread ocean acidification caused by anthropogenic CO_2. Kinetic data for the oxidation of pyrrhotite in seawater is just one piece of several that are missing in the characterization of SMS deposits and their interaction with seawater.

Kinetic experiments derive a rate law in the following fashion. For the reaction:

$$aA + bB \rightarrow cC + dD \qquad \text{Eq. 3}$$

The rate of reaction is defined as:

$$\text{Rate} = (-1/a)(dC_A/dt) = (-1/b)(dC_B/dt) = (1/c)(dC_C/dt) = (1/d)(dC_D/dt) \qquad \text{Eq. 4}$$

Which can be expressed as the rate law:

$$\text{Rate} = kC_A^{nA}C_B^{nB}C_C^{nC}C_D^{nD} \qquad \text{Eq. 5}$$

Where C is a unit of concentration, n is any real number and k is the rate constant (Lasaga, 1998). The negative signs indicate A and B are destroyed to create C and D.

Laboratory-based experiments are necessary to quantify sulfide mineral oxidation since *in situ* measurements are difficult (McKibben & Barnes, 1986; McKibben *et al*., 2008). There are two experimental approaches using reactors, as described by Brantley *et al*. 2008. Batch mode is the simplest setup which involves using a stirred reactor that is either open or closed to the atmosphere, and no new solution is introduced or removed. Reaction progress can be monitored through concentration changes over time by measuring the accumulation of reaction products in the vessel. Flow through reactors are also mixed continuously but allow the solution chemistry within the vessel to remain constant, as fluid flows constantly through the vessel and the cumulative effluent containing reaction products is sampled. The fundamental difference between batch and flow through mode is that seawater passes through the vessel (Brantley *et al*. 2008).

Current research in pyrrhotite geochemistry and oxidation is relevant in groundwater studies of acid mine drainage. Pyrrhotite is the second most common iron sulfide in nature (second to pyrite) and is a common waste mineral that will oxidize in an irreversible acid-producing reaction (Rxn. 1):

$$Fe_{(1-x)}S_{(s)} + (2-x/2)O_2 + xH_2O \rightarrow (1-x)Fe^{2+} + SO_4^{2-} + 2xH^+ \qquad \text{Rxn. 1}$$

$$Fe^{2+} + (1/4)O_2 + (5/2)H_2O \rightarrow Fe(OH)_{3(s)} + 2H^+ \qquad \text{Rxn. 2}$$

These reactions result in the acidification of surface and groundwater, precipitation of Fe^{3+} as ferric hydroxide (Rxn. 2) and increased mobility of trace metals in drainage waters (Belzile *et al*., 2004). The insoluble ferric hydroxide is the yellow and orange solid waste often seen downstream from mining activities (Kim *et al*., 1982).

The kinetics of these oxidation reactions has been evaluated in acidic groundwater specific to acid mine drainage from coal mining (Janzen *et al*., 1999, Nicholson & Scharer, 2000). Based on ferrous iron release, the mean oxidation rate of pyrrhotite by dissolved oxygen reported from Janzen *et al*. 2000 is $4x10^{-9}$ ($\pm$ $6x10^{-10}$) mol/m^2s. These results were obtained from experiments utilizing an internal split-flow airlift reactor at experimental conditions that range from 25-45^{o}C and pH 2-3 for grain sizes 125-180 μm.

Nicholson and Scharer (1994) used a pneumatically-driven mixed flow-through reactor to observe the oxidation of pyrite and pyrrhotite at pH = 2, 3, 4, 6 and 10^{o}, 22^{o} and 33^{o}C. The oxidation rate of pyrrhotite was 6-14$x10^{-9}$ mol/m^2s at 22^{o}C from pH 2-6 for 105 μm grains (the reaction was not strongly pH-dependent). A preferential retention of sulfur on grain surfaces was inferred with a possible correlation with an increase in pH, due to an observed decrease in the molar ratio of SO_4^{2-}/Fe with increasing pH in the effluent. Total dissolved Fe was a good indicator of the oxidation rate, however at pH >4 a chelating agent ethylenediaminetetra acetic acid (EDTA) was used to prevent the oxidation and precipitation of Fe^{2+}. However, both the precipitation and the use of a chelating agent could give an erroneously low rate of reaction.

2. EXPERIMENTAL DESIGN AND ANALYTICAL METHODS

This study mainly employs the initial rate method of deriving a rate law *via* batch reactor experiments, following McKibben and Barnes, (1984), Brantley *et al*., (2008), and McKibben *et al*., (2008). Several flow-through experiments were also conducted, but time did not permit a

comprehensive flow-through study, although preliminary flow-through results are reported in Appendix D.

2.1 EXPERIMENTAL DESIGN

Large, nearly pure pyrrhotite crystals were obtained from the Dal N'gorsk Primorsky Kray Mine, Far Eastern Region, Russia (Appendix A). Powder X-ray diffraction revealed the crystals to be monoclinic. Samples were roughly crushed to 1-5 mm size with the use of hammers and chisels and then hand-sorted for purity under a binocular 10x/20 microscope. The main impurities were galena, quartz and pyrite. Only the purest grains were used in experiments.

The purified grains were further crushed to a size fraction of 106-150µm or 45-106µm. Mineral powder left on prepared grain surfaces can give erroneously high dissolution rates (Holdren, 1981; Petrovich, 1981). Grain surfaces were cleaned to remove any fines and surface oxidation prior to experimentation. The importance of the surface preparation procedure is described in McKibben and Barnes (1986). Due to the slight magnetism of pyrrhotite, grains of adhering powder took longer to clean than for chalcopyrite grains (Bilenker, 2011) prior to use in experiments. Cleaning methods for grain surfaces included a combination of acid (chemical) cleaning and sonication (mechanical) cleaning. Approximately 1.1 g of pyrrhotite were sonicated up to five times with 40 mL of acetone for five minutes, decanting and rinsing with acetone in between sonications. Grains were then soaked in 1M HCl for ten minutes followed by an ethanol rinse. One to two more sonications with acetone were required after this to remove µm-sized grains from the surfaces of larger grains. Fig. 1a provides an SEM micrograph example of pre-cleaned grains and Fig. 1b shows grains after appropriate cleaning.

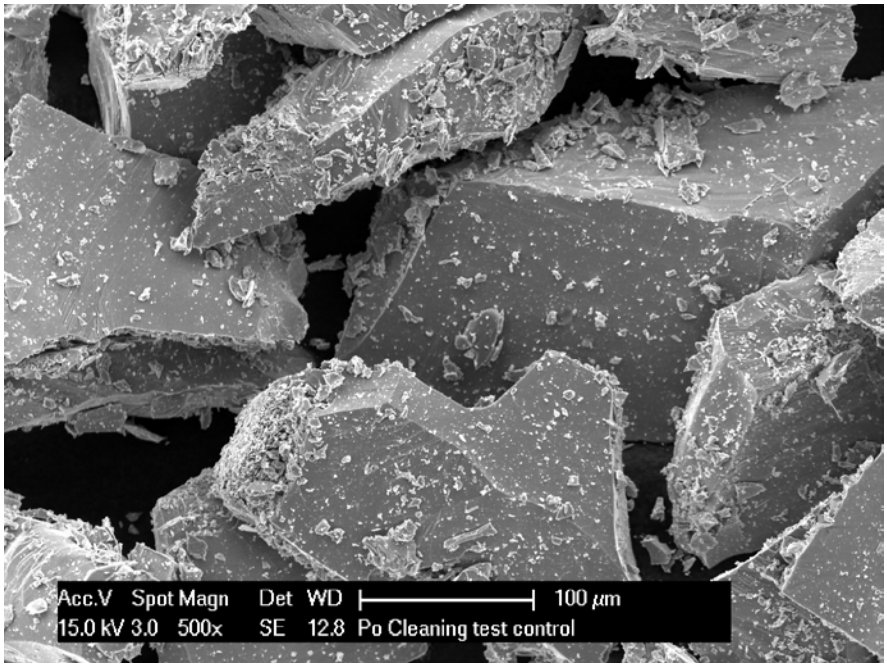

Fig 1a. Pyrrhotite grains after crushing and sieving, before cleaning

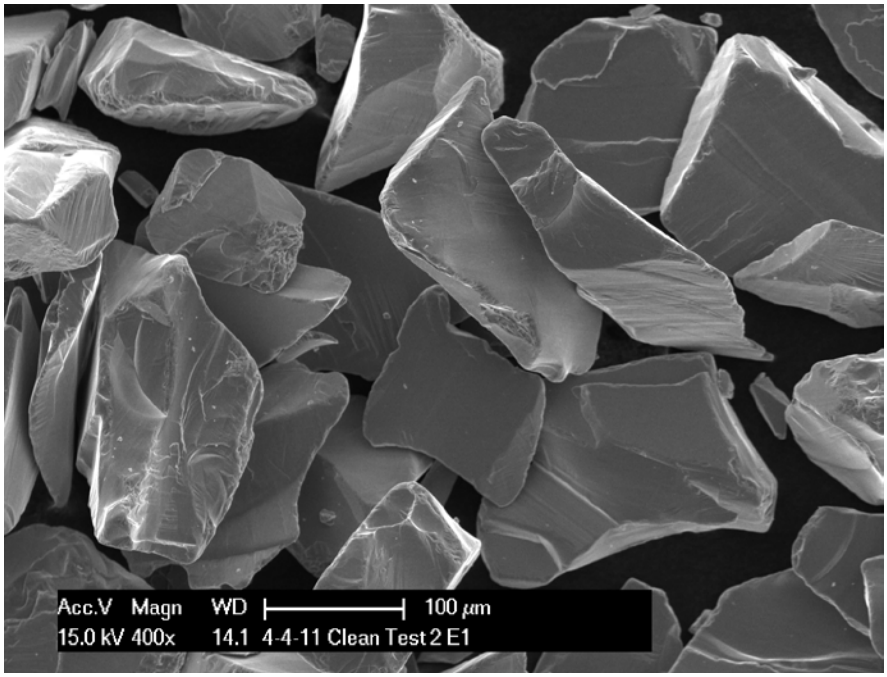

Fig 1b. Pyrrhotite grains after cleaning procedure completed

The grains were then dried in air before being loaded into the experiments. During the cleaning process approximately 0.1 g were lost during decanting.

Experimental set up was similar to McKibben and Barnes (1985) and McKibben *et al*. (2008). Up to two stirred Savillex Teflon reaction vessels (Model 101-2000-110-61) were placed inside a temperature-controlled heating-cooling circulation bath (Forma Scientific 2095 Bath & Circulator). Synthetic seawater was made following the formulation of Millero (2002). Dry salts were added by gram molar mass and hygroscopic salts were added volumetrically. The pH was adjusted with HCl and measured with a gel electrode (Thermo Scientific Orion 911600 Semi-Micro pH) designed for use in saline solutions.

Prior to experimentation in batch mode, the synthetic seawater was purged with either pure oxygen or a mixture of oxygen and nitrogen to maintain a fixed concentration of dissolved oxygen. Seawater was also equilibrated for temperature for experiments run outside of ambient temperature. After grains were cleaned, they were placed in a PVC sample platform between two pieces of nylon mesh (Appendix A). The sample platform was secured inside of a two-liter Teflon reaction vessel, which has ports for sampling, temperature measurements, gas inflow, and water inflow and outflow for closed-loop circulation. Vessels were placed inside temperature-controlled reactor baths for the duration of the experiment. The equilibrated seawater was funneled into the vessels using a separatory flask. To insure adequate fluid flow rates, the synthetic seawater in the vessel was mixed internally by pumping seawater through a closed loop using a Masterflex Economy Drive (Model 7554-90) and Easy Load Pump Head (Model 7518-00) rather than using a magnetic stirring device inside the vessel. Tracer dye tests indicated that at a pump rate of approximately 1050 mL/min, the fluid inside the vessel was

completely homogenized within 31 seconds. The start time of each experiment was considered to be the time at which the inflow from the circulatory pump first pumped seawater through the vessel. Stop time was immediately after the final sample was collected.

Oxidant transport is a potential limiting factor on oxidation rates. Before individual rate dependencies on environmental variables can be evaluated, identical experiments were run at different pump speeds to evaluate the effect of transport on the rate. Oxygen needs to be delivered to grain surfaces at a rate such that it is not limiting the rate of oxidation (Brantley, 2008).

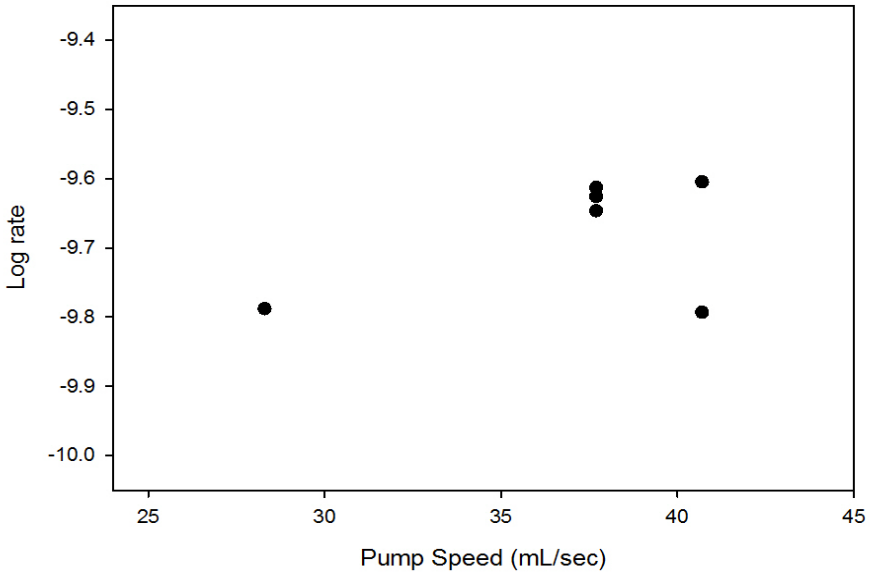

Fig. 2. Log Initial Rate vs. Pump Speed for runs at pH 3, 0.33 m^2/g, P_{O2} = 0.995, 20.0^{o}C. See Discussion for description of curve fitting for initial rate

Fig. 2 shows that at different pump speeds, the initial rate of reaction does not change significantly, which eliminates the issue of transport in this case.

A total of 1.8 L of seawater were used for each experiment, which ran for roughly 8 h. One mL samples were collected every thirty minutes, and more frequently at the start of each experiment. Including background samples taken for quality analysis/quality control, no more than 30 mL were removed from the vessel over the course of an experiment, decreasing the total volume in the vessel by less than 2%.

Upon completion of the experiments the initial rate of oxidation was calculated by fitting a second-order polynomial to the concentration vs. time data and taking the slope at time zero. The instantaneous measured rate could change as a function of time as the solution chemistry changes in the reactor. At the completion of each experiment pH was measured immediately.

Between runs, the experimental apparatus was cleaned using 2% Citranox (Alconox, Inc.), 2% Alconox (Alconox, Inc.), and rinsed five times with 18.2 MΩ ultrapure water. Experimental vessels were rinsed three times with ultrapure water, soaked in 5% HNO_3 for 24 hours, rinsed three times with ultrapure, and soaked for 24 hours in ultrapure between uses.

2.2 ANALYTICAL METHODS

The purity of pyrrhotite was confirmed by X-Ray Diffraction (XRD) (Shimadzu XRD 6000). Pyrrhotite is an unusual iron sulfide with varying iron contents. Due to these properties, pyrrhotite has monoclinic crystal structure but also hexagonal polytypes. XRD results of pyrrhotite used for experiments show measured 2θ peaks and intensities best fit pure monoclinic pyrrhotite for all peaks (Fig. 3). Although the exact polytype of pyrrhotite is not

differentiable from the spectrum, pyrrhotite is identified as having monoclinic crystal structure based on peak fit and intensity.

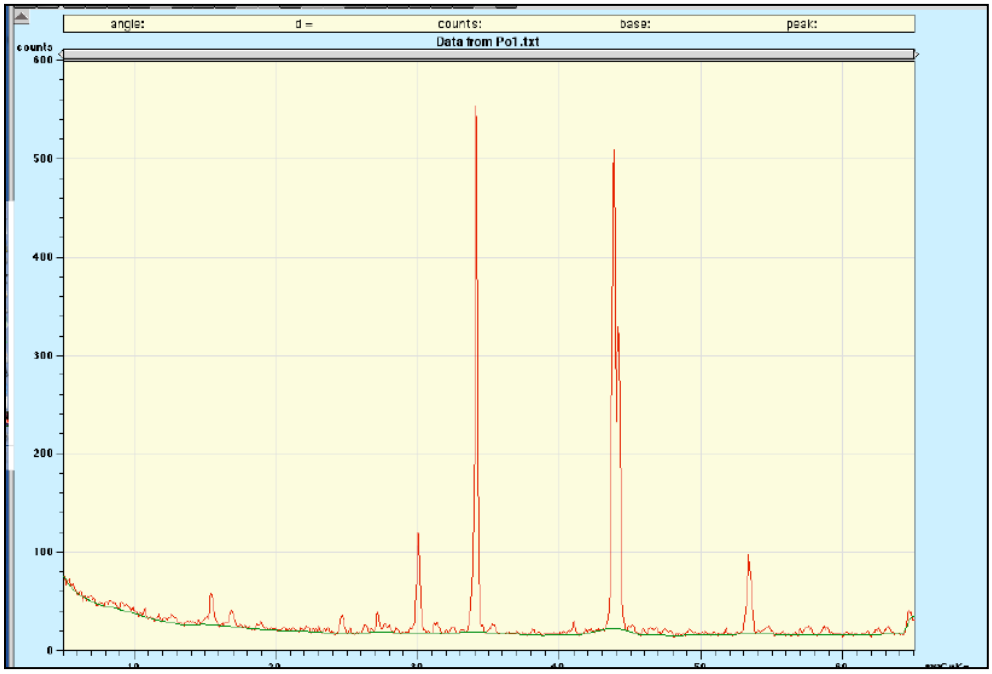

Fig 3. XRD spectrum for pyrrhotite (counts vs. 2θ)

Samples of the cleaned and prepared grains were sent to Quantachrome Instruments for surface area analysis with Krypton by the triple-point BET method (Fagurland, 1973). The surface area was measured to be 0.033 m^2/g for grain diameter 106-150 µm and 0.119 m^2/g for grain diameter 45-106 µm.

A Scanning Electron Microscope (SEM) (XL30-FEG) was used to evaluate the cleaning process by inspecting grain surfaces for adhering particulate matter. Energy Dispersive Spectroscopy (EDS) was used to further confirm purity. The software only displayed peaks for Fe and S for pyrrhotite samples (Fig. 4). The SEM was also used to analyze for any reaction

products remaining after completion of the run. Grain surfaces were inspected for any changes in topology (such as development of etch pits and eroded cleavages) and for reaction products that may have accumulated. The identity of any reaction product was confirmed using EDS.

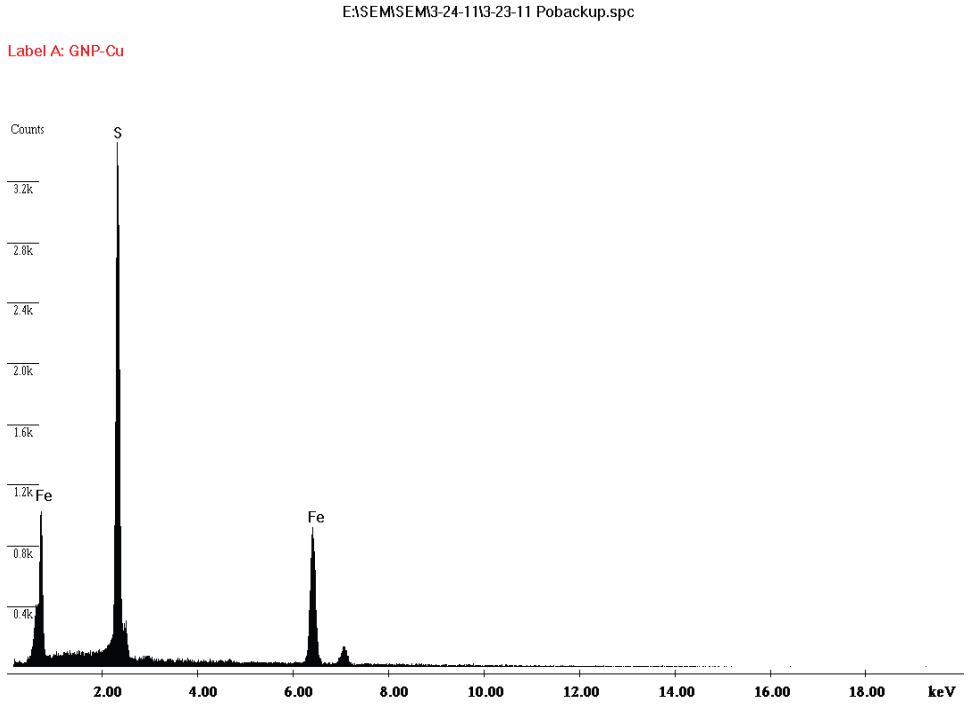

Fig 4. EDS spectrum of pyrrhotite (counts vs. keV) with S and Fe peaks identified

Fluid samples from the experiments were diluted ten-fold with 2% HNO_3 and analyzed on an Agilent 7500 Series (ICP-MS). Several different sets of standards were used depending on the range on Fe concentrations in the samples, and the standards themselves were not matrix-matched. Values are reported in parts per billion (ppb). Total dissolved Fe was used as the rate determining variable because the concentration of aqueous S contributed by the oxidation

reaction is impossible to differentiate at ppb concentrations, due to the high amount of background sulfate present in seawater.

3. RESULTS

Below are results from experiments summarizing the effect of each variable on the initial rate of oxidation of pyrrhotite in seawater. All experiments produced measurable Fe in solution (Fig. 5). The complete dataset is located in Appendix B.

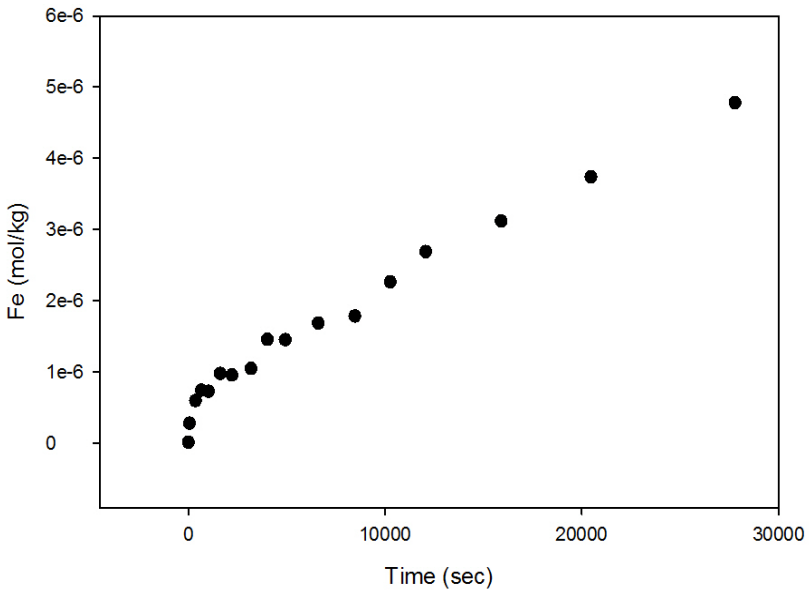

Fig 5. Typical run showing increased dissolved Fe with time at pH 3.0, 20.0°C, 0.033 m^2/g, P_{O2} = 0.995 atm

As oxidation progressed, total dissolved Fe increased. The individual effects of each important environmental variable on the oxidation rate are described below.

3.1 THE EFFECT OF pH

Runs were conducted at pH 2, 3, and 4 at 25°C, P_{O2} of 0.995 atm and grain size 106-150 µm. Runs above a pH of 4 showed irregular concentrations of Fe, and sometimes visible precipitates. Precipitates were white in color, and occasionally there was iron staining observed on the mesh of the sample platform. The chemical composition of the precipitates could not be identified due to an insufficient mass of material to analyze by XRD. Batch mode runs conducted at seawater pH did not have a measurable decrease in pH, but rather an overall increase over time, potentially caused by the formation of precipitates on grain surfaces preventing further dissolution of iron and release of protons (Nicholson & Scharer, 1994); however, this was not observed directly. Experiments with starting pH 7.5 after eight hours increased to pH 8.2 or higher (Table 1).

Run	Starting pH	Final pH
P040	7.54	8.81
P041	7.56	8.91

Table 1. Starting and ending pH for runs >pH 7.0

Two experiments were run for three days had final pH's >9.0. Data shows erratic concentrations of Fe in solution during the experiments. Iron staining was also visible on the mesh containing the pyrrhotite at experiment completion.

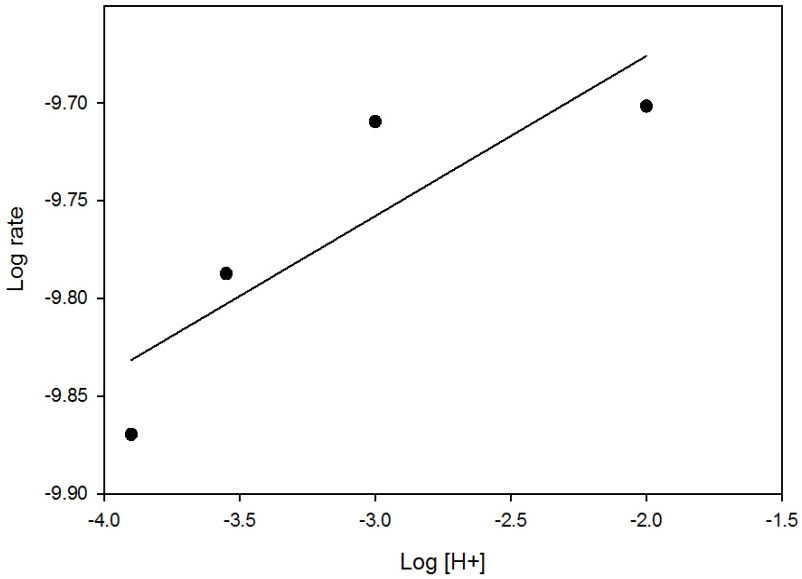

Fig. 6. Log initial rate versus log proton concentration

Dependence of pH can be extrapolated at higher pH using Fig 6. The slope of the line in Fig. 6 is -0.08 ± 0.0.03 and compared with other variables, the effect of pH on the rate is minimal.

Grain surfaces post-reaction were observed with SEM. Due to the irregular topography of the grains, it was difficult to collect a reliable EDS spectrum, however, there is a large oxygen peak that is not present on unreacted pyrrhotite grains from runs at higher pH. It is possible that an oxidative coating develops early in the reaction, preventing grains from further dissolution. Precipitates may be less of an issue in the flow-through experimental setup since reaction products accumulate outside of the vessel, instead of in samples.

No significant changes in pH were observed over the duration of runs at pH ≤ 4. This is not surprising at lower pH because there would need to be a large amount of proton production

to drive a low pH even lower. Runs conducted at higher pH where precipitates were either observed or inferred had higher final pH's than initial pH's.

3.2 EFFECT OF SURFACE AREA

Two different grain sizes (45-106 μm and 106-150 μm) were examined to determine the effect of surface area on the initial rate. Pyrrhotite grains with size distribution of 45-106 μm have a surface area of 0.119 m^2/g, and pyrrhotite grains with size distribution of 106-150 μm have a surface area of 0.033 m^2/g. For the given total mass, higher specific surface area (smaller diameter) grains oxidize more quickly than lower specific surface area grains, which has a positive influence on the rate. Several experiments were also conducted at lower specific surface area (grain size 150-180 μm); however due to the expensive cost of the BET analysis, surface area measurement was not completed on this grain size.

Surface area is also used to calculate the specific rate (R_{sp}), from which the specific rate constant k is calculated:

$$-dM_{Fe(1-x)S} / dt = k (A/V) (M_{O2})^a (M_{H+})^b \quad \text{Eq. 6}$$

$$R_{sp} = k (M_{O2})^a (M_{H+})^b \quad \text{Eq. 7}$$

where A is total mineral surface area, V is the volume of seawater, and a and b are reaction orders for the molar aqueous species' concentrations (M). Runs performed at 0.119 m^2/g had initial rates approximately 1.74 times faster than those ran at 0.033 m^2/g (Appendix A).

3.3 OXIDANT CONCENTRATION

Oxygen mixed with nitrogen was used in runs to explore the effect of oxidant concentration on the rate. Runs were conducted at different P_{O2} values (0.995 atm, 0.100 atm, and 0.010 atm) at 25°C, pH 3, and 106-150 µm grain size.

Seawater has a low capacity for oxygen absorption due to the salting out effect (Benson & Krause, 1984). Dissolved oxygen (C^*_o) is calculated with the following equation from Garcia and Gordon (1992) (Simplified from Benson & Krause, 1984):

$$C^*_o = 0.20946\ F(1-P_{wv})\ (1-B_o)\ (K_oM_w)^{-1} \qquad \text{Eq. 8}$$

where 0.20946 is the mole fraction of O_2 in dry air (which will be substituted with experimental values of P_{O2}), F is the salinity factor (35 from Millero, 2002), P_{wv} is the vapor pressure of water in air, B_o is the second virial coefficient for O_2 (from Benson & Krause, 1980), K_o is Henry's law coefficient for O_2 in seawater, and M_w is the molecular mass of water. Computations for each temperature and P_{O2} are located in Appendix C.

Increased concentrations of oxygen have a positive effect on the rate of oxidation, as expected. However, the difference between 0.100 atm and 0.995 atm O_2 was not nearly as significant as the difference between 0.010 atm and 0.100 atm O_2 (Fig. 7). This suggests that the effect of O_2 concentration on the rate may not be linear over the P_{O2} range used.

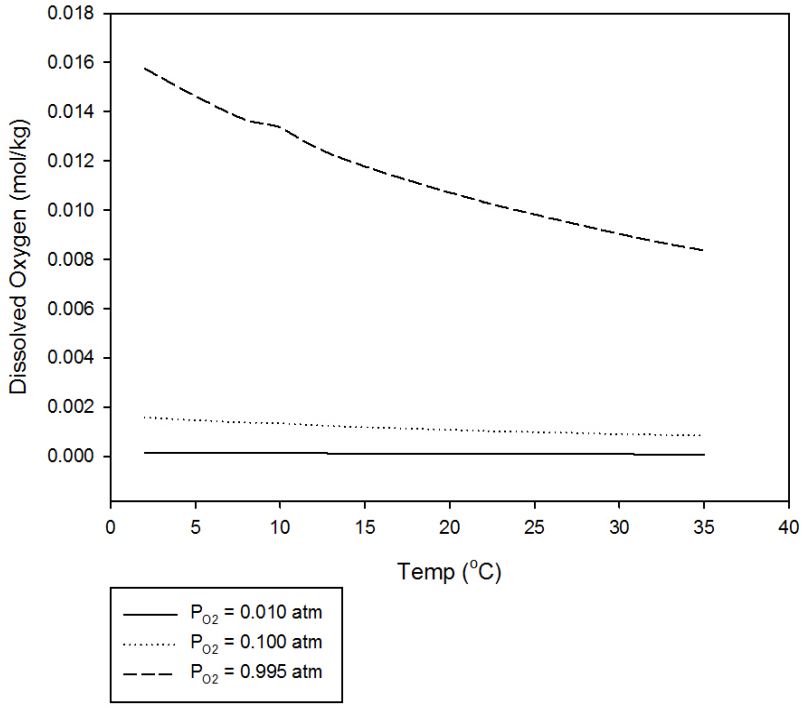

Fig. 7. Dissolved oxygen (mol O_2/kg seawater) vs. Temperature (^{o}C) for seawater density 1.025 kg/dm^3

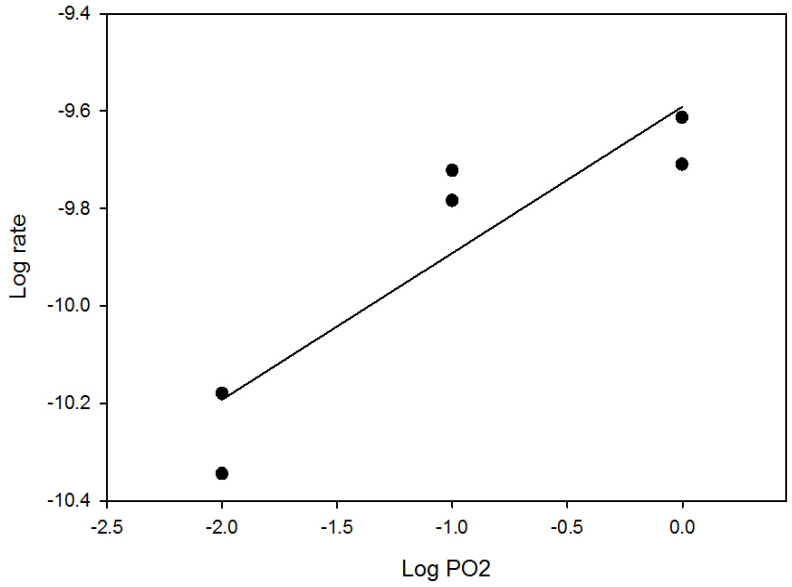

Fig. 8. Log initial rate vs. log P_{O2} for runs at pH 3, 20.0°C, 0.033 m^2/g

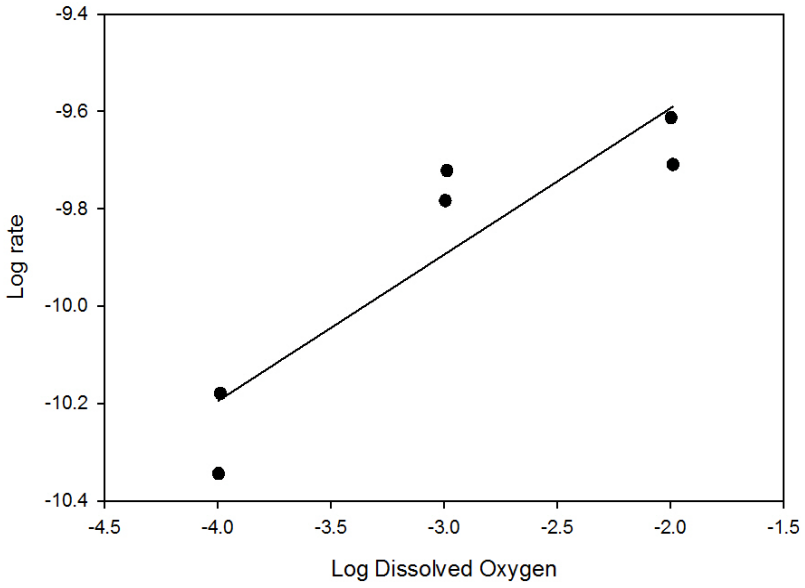

Fig. 9. Log initial rate vs. Log DO for runs at pH 3, 20.0°C, 0.033 m^2/g
The slope of line in Fig. 9 is 0.3008 ± 0.0.0699.

3.4 EFFECT OF TEMPERATURE

Temperature has the most significant affect on the rate. Runs were conducted at conditions as low as 4°C and as high as 35°C. These temperatures represent the practical experimental limits of the equipment, but rates at slightly lower and higher temperatures can be extrapolated with linear regression of the data with inverse temperature (Fig. 10). Runs conducted over 35°C caused seawater to evaporate at a sufficiently rapid rate such that the loss in volume significantly affected the rate.

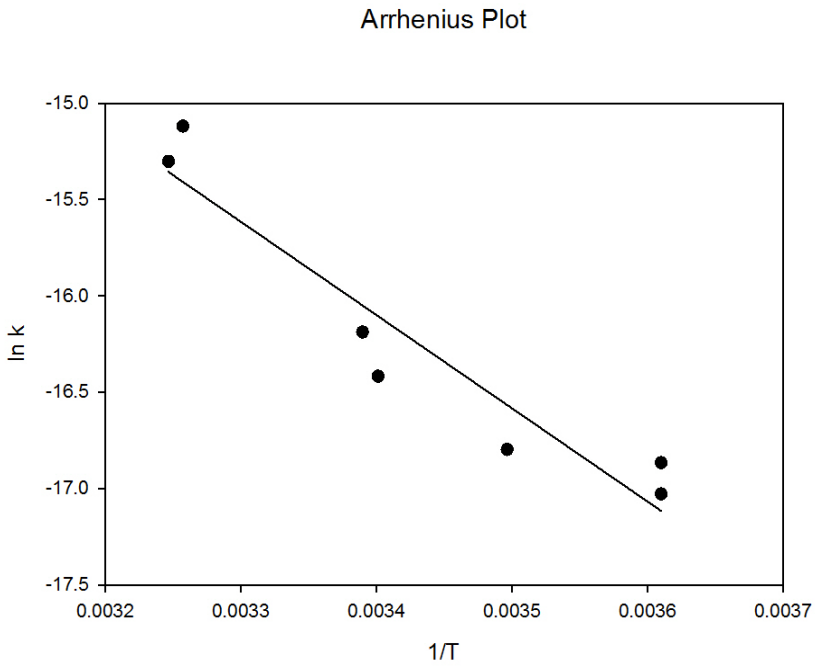

Fig 10. Arrhenius plot for the natural log of rate constants k vs. 1 over absolute temperature.

The effect of temperature on the rate is traditionally determined with the Arrhenius plot (Fig. 10), the natural log of the specific rate constant versus the inverse absolute temperature, for fixed concentrations of $[H^+]$ and O_2. The activation energy as calculated from the Arrhenius plot is 40.26 kJ/mol.

Dissolved oxygen (DO) is also dependent on the density of seawater, which is affected by pressure. DO calculations were completed for a seawater density of 1.025 kg/dm^3 for surface seawater, and 1.050 kg/dm^3 for seawater at 1500 m depth. The minor change in seawater density had little effect on the resulting dissolved oxygen output. Appendix B contains data from DO calculations.

4. DISCUSSION

The results above and in Appendix B were used to construct a specific rate law for pyrrhotite oxidation in seawater employing the initial rate method (Lasaga, 1998) in conjunction with the isolation method (McKibben *et al*. 2008; McKibben & Barnes, 1986). Fe was used as the rate determining variable since high natural background concentrations of SO_4^{2-} in seawater would make ppb changes in total dissolved S due to sulfide mineral dissolution indistinguishable. Using the isolation method, the initial amounts of one reactant or product are varied while all other variables are held constant. Following the differential method (Lasaga, 1998) for each run a second-order polynomial in the form $M_i = x + yt + zt^2$ was fit to the data for total dissolved Fe

per unit time using the program SigmaPlot™ (Appendix B). The slope of the second-order polynomial is found at t = 0 by taking the first derivative of M. This is the initial reaction rate.

The isolation method (e.g. Bilenker, 2011; McKibben *et al*., 2008; McKibben & Barnes, 1986) was employed to evaluate the effects of each variable on the rate (Eq. 5). By adjusting one variable at a time, we can evaluate the relation between the rate and that particular reactant or product (Lasaga, 1998). The variables in this case are the molar concentrations of O_2 and H^+ and the temperature. The coefficients n (Eq. 5) can be deduced from taking the log of the rate. Figs. 6 and 10 show the log initial rates vs. log $[H^+]$ and log DO, respectively. The curve fit in these plots represents the reaction order for each of these variables, again, 0.08±0.03 and 0.30±0.07, respectively. The effects of mineral surface area, solution volume, and mass of mineral used in each run are incorporated when the initial rate becomes the specific rate (Eq. 9 and 10).

The derived volumetric rate law is as follows:

$$R_{vol(Fe(1-x)S)} = -k\,(A/V)\,(M_{H+})^{0.08\pm0.03}\,(M_{O2(aq)})^{0.30\pm0.07} \qquad \text{Eq. 9}$$

where R_{vol} is in mol/L sec. Multiplication by V/A gives the specific rate law:

$$R_{sp(Fe(1-x)S)} = -k\,(M_{H+})^{0.08\pm0.03}\,(M_{O2(aq)})^{0.30\pm0.07} \qquad \text{Eq. 10}$$

wher R_{sp} is in mol/m^2 sec. The average rate constant k in $mol^{0.68}\ L^{0.32}/m^2$ s for runs at 22.0°C is 5.38×10^{-8}. The complete list of k's for all runs is located in Appendix B.

4.1 THERMODYNAMIC MODELING

Thermodynamic reaction progress modeling of the runs with the Geochemist's Workbench (GWB) predicts iron hydroxide precipitation early in the reaction at seawater pH values, followed ultimately by jarosite precipitation as the pyrrhotite is completely consumed (reaction progress 1.0). (Fig. 11).

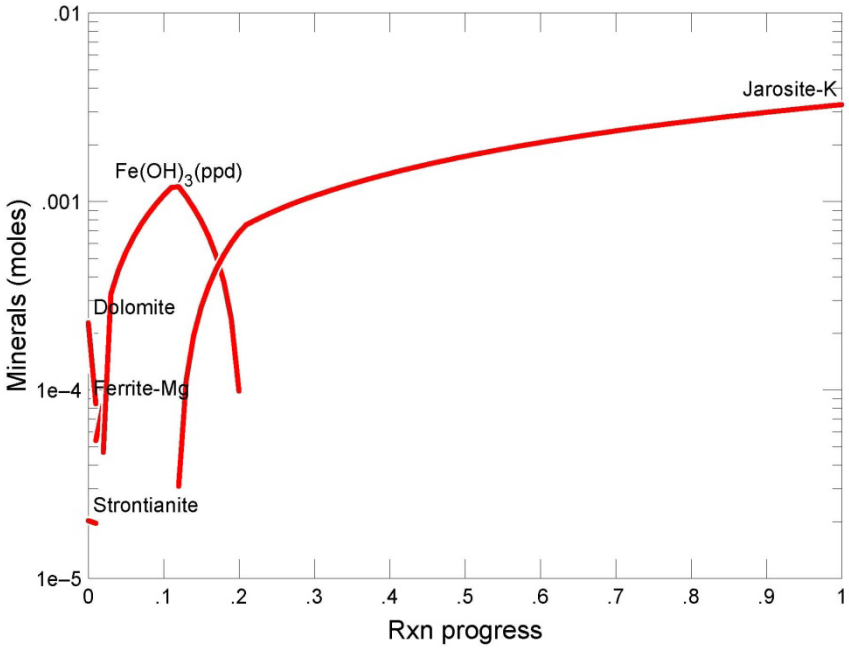

Fig 11. GWB model reacting pH 7.5 seawater with 1 g of pyrrhotite at 20.0°C where P_{O2} = 0.995 atm

GWB also predicts that starting at a seawater pH of 7.5, the complete oxidation of 1 g of pyrrhotite in 1.8 L of seawater eventually produces enough protons to bring the final pH below 3 (Fig. 12). However, none of our runs were conducted long enough (weeks or months) to go to completion, so the precipitation of jarosite would not have been attained and the pH was not observed to drop so low.

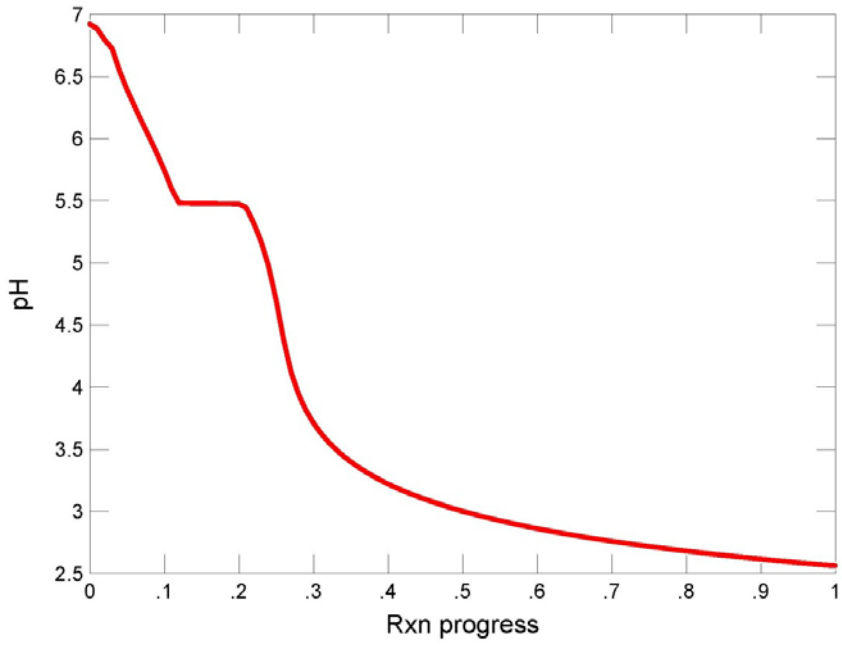

Fig 12. GWB predicted changes in pH

In fact, the actual runs conducted at initial seawater pH did not show an expected decrease in pH after 8 hours, but rather a slight increase up to pH 8.5, indicating that some other unexpected reaction is taking place or precipitates form during pyrrhotite oxidation and prevent significant further solubilization of Fe.

It is possible to predict sulfuric acid production from pyrrhotite oxidation by molar relationships alone. There are several different possible reactions that could take place on the seafloor. Geochemist's Workbench predicts both Fe hydroxide and jarosite precipitation. The following reactions were written in terms of these products using Geochemist's Workbench:

$$\text{pyrrhotite} + 2.375\ H_2O + 2.313O_{2(aq)} + 0.5\ K^+ + 0.625\ Fe^{2+} \rightarrow 0.5\ \text{jarosite-K} + 1.75\ H^+ \qquad \text{Rxn. 3}$$

$$\text{pyrrhotite} + 2.313\ H_2O + 2.156\ O_{2(aq)} \rightarrow 2H^+ + 0.875\ Fe(OH)_3 + SO_4^{2-} \qquad \text{Rxn. 4}$$

Using reaction stoichiometry for Rxn. 3, every kg of pyrrhotite reacted produces 2.70 mg of protons. In Rxn. 4, for every kg of pyrrhotite, 3.09mg of protons are produced.

Seawater is an excellent buffer for changes in pH. The buffer capacity (B_c) is defined as the threshold at which a solution is able to resist changes to pH (Eq. 11) and is a function of chlorinity (Cl) (Thompson & Bonnar, 1931):

$$B_c/Cl = 0.1252 \qquad \text{Eq. 11}$$

The Millero formulation of seawater used in experimentation has a chlorinity of 19.4‰, which makes the buffer capacity 6.5. This is the threshold number of grams of acid per kilogram of seawater before changes in pH will occur. Predictions from both Rxns. 4 and 5 are well within the buffer capacity for seawater.

The Geochemist's Workbench modeling has some discrepancies. The model predicts that total consumption of pyrrhotite during oxidation in seawater will have a significant drop in pH (Fig. 12). However, the reactions written with the program using the same reactants do not produce large amounts of protons when the buffer capacity is calculated by hand. Although

molar relationships do not predict enough acid production to drive the local seawater pH down, experiments were not run long enough to observe and measure this empirically. Since a slight increase in pH was observed in experiments at pH 5 and above, hydroxide production may initially exceed proton production; however, if the reaction were to run to completion proton production would still not exceed hydroxide production by molar predictions. It is also possible that at higher pH an oxidative coating develops on pyrrhotite grains early on in the reaction preventing further dissolution of Fe and release of protons. This phenomenon has been demonstrated in pyrite (Nicholson *et al*., 1990) and inferred as a possibility during pyrrhotite oxidation in freshwater (Nicholson & Scharer, 1994).

There are other factors that were not evaluated during this study that will play a role in acid production from seafloor mining. For example, the SMS material ground *in situ* will be slurried up to a mining support vessel on the surface for rough processing (Hoagland *et al*., 2010). During this time the material will be further crushed, creating higher surface area and exposing particles with fresh, unreacted surfaces. These grain surfaces will experience both higher temperatures and concentrations of oxygen at the surface and each of these factors accelerates oxidation.

Following shipboard processing, waste effluent containing grains smaller than 8 µm in diameter will be pumped to depth and released just above the seafloor (Gwyther, 2008). The fate of these particulates is not dissimilar to that of natural vent particulates from the active hot spring vents, so consideration is also warranted of potential acid production from such sulfide particulates.

In other words, we should consider how long pyrrhotite grains will last near the seafloor, as either natural vent particulates or mining products. The "shrinking sphere model" from Hume and Rimstidt (1992), which was adapted by Jurinski (1998), can be used to evaluate how long it would take for a grain of pyrrhotite to completely oxidize at the seafloor. The following equation defines the amount of time it takes a spherical grain to completely disappear under conditions controlled by the specific rate constant:

$$\Delta t = d / 2V_m k \qquad \text{Eq. 12}$$

where t is time, d is the diameter of a spherical grain, V_m is the molar volume, and k is the specific rate constant. Since this equation was derived for a zeroth order reaction, to adapt for the pyrrhotite oxidation reaction R_{sp} (mol/m^2 sec) was substituted for k which has non integer units$mol^{0.68}L^{0.32}$ / m^2 s .As previously mentioned, at seawater pH the quantification of pyrrhotite oxidation rates is hindered by the formation of precipitates. But using the rate of pH 3 experiments with P_{O2} = 0.010, the time for a pyrrhotite grain of 8 µm would take approximately 2 years 10 months to be completely consumed. Calculations were performed using Eq. 12, R_{sp} value from run P073 (Appendix B), and the $V_{m(Po)}$ 17.58 cm^3/mol (Robie *et al* 1979):

$$d/2V_mR_{sp} = 8\ \mu m / 2[\ (1.758 \times 10^{13}\ \mu m^3/mol)\ (2.5337 \times 10^{-21}\ mol/\ \mu m^2\ sec)]$$

$$\Delta t = 8.980 \times 10^7\ sec \approx 2\ years\ 10\ months$$

The actual time would likely be longer than this since experiment P073 was conducted at 23.0^oC to generate R_{sp} used in the model.

Oxidation by bacteria also plays a role in sulfide oxidation. Bacteria generally accelerate the oxidation process, and certain chemolithotrophic microorganisms can accelerate oxidation by a factor of up to 10^6 (Rawlings, 1997). The effect of bacteria on sulfide oxidation in seawater is currently unknown but would be an important effect to quantify for natural in situ SMS oxidation. On a seafloor mining time scale, however, bacterial catalysis of oxidation may be insignificant.

Advective and diffusive transport of ocean currents also contribute to the sphere of influence of mining activities on the seafloor. The rate law, when incorporated into reactive transport computer models, may be able to predict how long iron sulfide particulates in both natural vent plumes and anthropogenic mining discharge plumes might persist. Some modeling has been done with mixing between hydrothermal solutions from black smokers and seawater simulating mineral precipitation nearby seafloor vents (Janecky & Seyfried, 1984). Thermodynamic data and reaction modeling codes could be accommodated to mining activity to predict the nature and persistence of waste material.

5. CONCLUSIONS

Acid mine drainage (AMD) is a serious environmental problem that affects plant and animal life, mine productivity, and profitability of terrestrial operations. Lessons learned from AMD have encouraged better and more environmentally-conscious mining operations. It is important to perform studies before AMD occurs; it is easier to prevent a problem than to clean one up.

Results from this study are akin to the natural weathering rates of SMS deposits since only pH, temperature, surface area and P_{O2} were evaluated with respect to the rate of oxidation, and many of the mining specific processes mentioned in the Discussion were not modeled in the laboratory. Several conclusions have been drawn: At low pH the abiotic oxidation of pyrrhotite in seawater is affected positively by increasing temperature, surface area, and concentrations of O_2 and H^+.

1. The rate of oxidation is most significantly affected by temperature and consequently by oxidant concentration due to the salting out effect.
2. Above pH 4.5, the release of Fe is hindered by the production of Fe-OH precipitates.
3. The rate of this reaction can be considered an upper limit for sulfide oxidation on the seafloor.
4. The buffer capacity of seawater will not be exceeded due to sulfuric acid production.

The implications are promising for the seafloor mining industry; it is unlikely that seafloor acid mine drainage will occur from mining activities. Although at low pH the rate is affected positively by increasing temperature, surface area, and concentrations of O_2 and H^+, at seawater pH the reaction is hindered by the formation of precipitates. Even as an upper limit for sulfide oxidation, pyrrhotite oxidized completely would not theoretically produce enough protons to exceed the buffer capacity of seawater.

There is plenty of potential for future work on this topic. Several flow-through experiments were run with pyrrhotite but time did not permit for an entire flow-through study. Preliminary results from flow-through experiments are reported in Appendix D. Rate laws also

need to be developed for other SMS minerals like galena and sphalerite, as well as sulfate minerals formed at white smokers like gypsum and anhydrite. A study of bacterial catalysis would also provide more information on the real effects of sulfide mineral oxidation on seafloor ecology.

This industry is developing rapidly due to the demand and high price of copper and gold currently, however in light of this, it is important that we are able to identify and control the effects on the environment.

6. REFERENCES

Belzile, N., Chen, Y-W, Cai, M-F, Li, Y., 2004, A review on Pyrrhotite Oxidation, Journal of Geochemical Exploration, 84, 65-76

Benson, B.B. and Krause, D. (1980) The concentration and isotopic fractionation of gases dissolved in freshwater in equilibrium with the atmosphere. 1. Oxygen. Limonl. Oceanogr. 95(4): 662-671

Benson, B.B. and Krause, D. (1984) The concentration and isotopic fractionation of oxygen dissolved in freshwater and seawater in equilibrium with the atmosphere. Limonol. Oceanogr. 29(3): 620-632.

Bilenker, L.D., 2011, Abiotic oxidation rate of Chalcopyrite in seawater: implications for seafloor mining, University of California, Riverside Press

Blodau, C. 2006. A review of acidity generation and consumption in acidic coal mine lakes and their watersheds. Science of the Total Environment 369 (1-3), 307-332.

Brantley, S.L., Kubicki, J.D., White, A.F., 2008, Kinetics of Water Rock Interaction, Springer Science + Business Media, LLC

Davis, E.E., Mottl, M.J., Fisher, A.T., et al., 1992. *Proc. ODP, Init. Repts.,* 139: College Station, TX (Ocean Drilling Program).

Duckworth, J.R.H., 1998, Drilling of Sediment Hosted Massive Sulphide deposits at the Middle Valley and Escanaba Trough spreading centers: ODP Leg 169, Modern Ocean Floor Processes and the Geologic Record

Fagurland, G., 1973, Determination of specific surface by the BET method, Materials and Structures, 6, 239-245

Fornari, D.J., Embly, R.W., 1995, “Tectonic and Volcanic Controls on Hydrothermal Processes at the Mid-Ocean Ridge: An Overview Based on Near-Bottom and Submersible Studies,” Seafloor Hydrothermal Systems: Physical, Chemical, Biological, and Geological Interactions: American Geophysical Union pp. 1-46

German, C.R., Sparks, R.S.J., 1993, Particle recycling in the TAG hydrothermal plume, Earth Planet. Sci. Lett., 116, 129-134

German, C.R., Baker, E.T., Klinkhammer, G., 1995, Regional Setting of Hydrothermal Activity, Hydrothermal Vents and Processes, Geological Society Special Publication No. 87, 3-15

Garcia, H.E., Gordon, L.I. (1992) Oxygen solubility in seawater: Better fitting equations. Limnology and Oceanography 37(6): 1307-1312

Gwyther, D., Wright, M., 2008, Environmental Impact Statement: Solwara 1, Coffey Natural Systems Pty Ltd, 47-65

Heilig, G. K., Gerland, P., Andreecv, K., Li, N., Gu, D., Spoorenberg, T., Ravinuthala, S., Yamarthy, C., Koshy, N. 2012. Population estimates and projection section: work program, outputs, challenges, uncertainties. United Nations Department of Economic and Social Affairs, www.unpopulation.org Helfrich, K.R., Speer, K.G., 1995, "Oceanic Hydrothermal Circulation: Mesoscale and Basin-Scale Flow," Seafloor Hydrothermal Systems: Physical, Chemical, Biological, and Geological Interactions: American Geophysical Union

Hoagland, P., Beaulieu, S., Tivey, M.A., Eggert, R.G., German, C., Glowka, L, Lin, J., 2010, Deep-sea mining of seafloor massive sulfides, Marine Policy, 34, 728-732

Hoffert, J.R., 1947,Acid Mine Drainage, Ind. Eng. Chem., 39 (5), pp 642–646

Holdren, G.R., 1981, Fine particle dissolution behavior and its effect on the apparent dissolution kinetics of primary silicate minerals (abstr.), Geol. Sec. Amer., Prog. 13, 475Hume, L.A., Rimstidt, J.D., 1992, The biodurability of chrysotile asbestos, The American Mineralogist, Vol: 77, 9-10, 1125-1128

Janecky, D.R., and Seyfried, W.E. (1984) Formation of massive sulfide deposits on oceanic ridge crests: Incremental reaction models for mixing between hydrothermal solutions and seawater, Geochimica et Cosmochimica Acta, 48, No. 12, 2723-2738

Janzen, M.P., Nicholson, R.V., Sharer, J.M., 1999, Pyrrhotite Reaction Kinetics: Reaction rates for oxidation by O_2, Fe^{3+}, and non-oxidative dissolution, Geochimica et Cosmochimica Acta, 64, No. 9, 1511-1522

Johnson, D.B., 2003, Chemical and microbiological characteristics of mineral spoils and drainage waters at abandoned coal and metal mines, Water Air Soil Pollution, No. 3, 47-66

Johnson, D.B., Hallberg, K.B., 2005, Acid mine drainage remediation options: a review, Science of the Total Environment, 338, 3-14

Jurinski, J.B., 1998, Geochemical Investigations of Respirable Particulate Matter, Virginia Polytechnic Institute and State University Press

Kim, A.G., Heisey, B.S., Kleinmann, R.L.P, Deul, M., 1982, Acid Mine Drainage: Control and Abatement Research, Series: Information circular (United States. Bureau of Mines), No. 8905, 1-22

Lasaga, A.C., 1998, Kinetic Theory in the Earth Sciences: Princeton University Press

Loudin, G., 2011, Annual Report, Nautilus Minerals, Inc., 6

Lupton, J.E., J.R. Delaney, H.P. Johnson, M.K. Tivey, 1985, Entrainment and vertical transport of deep ocean water by hydrothermal plumes, Nature No. 316, 621-623

McBeth, J. M., B. J. Little, R. I. Ray, K. M. Farrar, and D. Emerson, 2011, Neutrophilic iron-oxidizing "Zetaproteobacteria" and mild steel corrosion in nearshore marine environments. Applied and Environmental Microbiology 77:1405-1412.

McKibben, M.A., Barnes, H.L., 1986, Oxidation of pyrite in low temperature acidic solutions: Rate laws and surface textures, Geochimica et Cosmochemica Acta Vol. 50, WI. 1509-1520

McKibben, M.A., Tallant, B.A., del Angel, J.K., 2008, Kinetics of inorganic arsenopyrite oxidation in acidic aqueous solutions, Applied Geochemistry, No. 23, 121-135

Millero, F.J. (2002) Chemical Oceanography. CRC Press LLC, Boca Raton, pp 65

Mills, R.A., 1995, “Hydrothermal Activity and the Geochemistry of Metalliferous Sediment,” Seafloor Hydrothermal Systems: Physical, Chemical, Biological, and Geological Interactions: American Geophysical Union

Mills, R.A., 1995, “Hydrothermal deposits and metalliferous sediments from TAG, 26^{o}N Mid-Atlantic Ridge, Hydrothermal Vents and Processes: Geological Society Special Publication No. 87, 121-132

Misra, K.C., 2012, Introduction to Geochemistry: Principles and Applications, First Edition, Blackwell Publishing Inc., 197-221

Mottl, M.J., T.F. McConachy, 1990, Chemical processes in buoyant hydrothermal plumes on the East Pacific Rise near 21^{o}N, Geochim. Cosmochim. Acta, No. 54, 1911-1927

Nicholson, R.V., Sharer, J.M., 1994, Lab Studies of Pyrrhotite Oxidation Kinetics, Environmental Geochemistry of Sulfide Oxidation, ACS Symposium Series 550, 14-30

Nicholson, R.V., Gillham, R.W., Reardon, E.J., 1990, Reactivity of the (100) Plane of Pyrite in Oxidizing Gaseous and Aqueous Environments: Effects of Surface Imperfections, Geochim. Cosmochim. Acta, 54, 395-402

Petrovich, R., 1981, Kinetics of dissolution of mechanically comminuted rock-forming oxides and silicates. I. Deformation and dissolution of quartz under laboratory conditions, Geochim. Cosmochim. Acta 45, 1665-1674

Rawlings, D. E. (ed.): 1997, Biomining: Theory, Microbes and Industrial Processes. SpringerVerlag/Landes Bioscience, Georgetown, Texas, U.S.A., 302

Robie, R.A., Hemingway, B.S., Fisher, J.R. (1979) Thermodynamic Properties of Minerals and Related Substances at 298.15 K and 1 Bar (10^5 Pascals) Pressure and at Higher Temperatures, U.S. Geological Survey Bulletin 1452, United States Government Printing Office, Washington, 17

Rudnicki, M., Elderfield, H., 1993, A chemical model of the buoyant and neutrally buoyant plume about the TAG vent field, Mid-Atlantic Ridge, Geochim. Cosmochim. Acta, No. 57, 2939-2957

Simón, M., Ortiz, I., Garcia, I., Fernández, E., Fernández, J., Dorronsoro, C., Aguilar, J., 1999, Pollution of soils by the toxic spill of a pyrite mine (Anzalcollar, Spain), Science of the Total Environment, 242, 105-115

Speiss, F.N., et al., East Pacific Rise: Hot Springs and geophysical experiments, Science, No. 207, 1421-1433

Stommel, H., 1982, Is the south Pacific Helium-3 plume dynamically active?, Earth Planet, Sci. Lett., No. 61, 63-67

Tallant, B.A., (2005) Kinetic Rate of Arsenopyrite Dissolution by Oxygen in Low Temperature, Low pH Solutions. Unpublished M. Sc. Thesis, University of California, Riverside.

Thompson, T.G., Bonnar, R.U., 1931, The buffer capacity of sea water, Ind. Eng. Chem. Anal. Ed., Vol 3 No. 4, 393–395

Von Damm, K.L., 1995, “Controls of the Chemistry and Temporal Variability of Seafloor Hydrothermal Fluids,” Seafloor Hydrothermal Systems: Physical, Chemical, Biological, and Geological Interactions: American Geophysical Union

APPENDICES

Table of Contents

List of Figures

List of Tables

1. **APPENDIX A:** Batch experiment setup

Fig. 1. Pyrrhotite crystal from the Dal N'gorsk Primorsky Kray Mine, Far Eastern Region, Russia

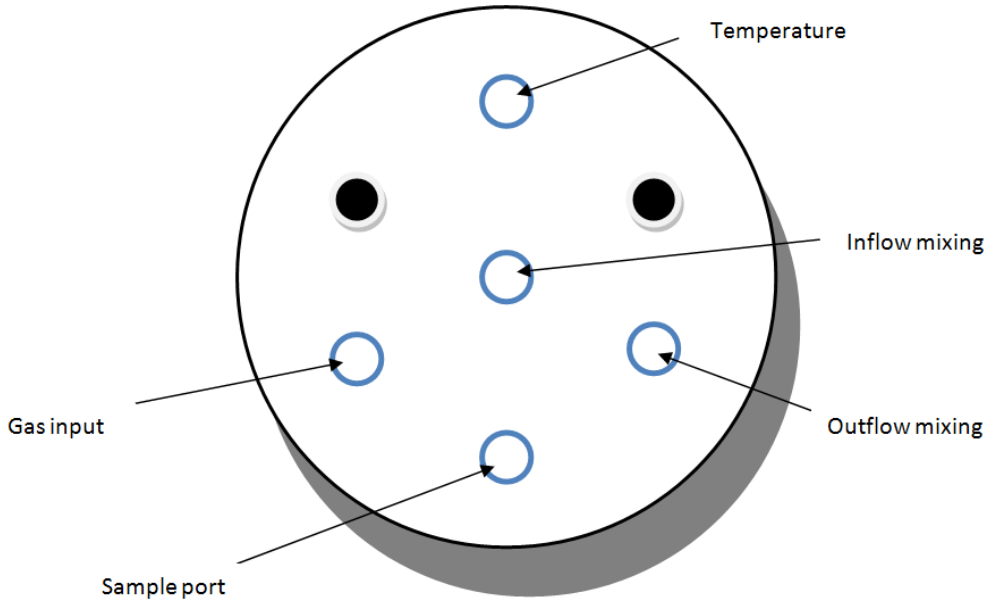

Fig. 2. Top of 2L Teflon vessel showing ports for inflow and outflow, gas, temperature, and sample collection

Fig. 3. Sample platform

Fig. 4. Two experiments set up in temperature controlled reactor bath with Teflon balls and ethylene glycol for insulation

2. APPENDIX B: Experimental Data

2.1 Run conditions for experiments incorporated into rate law and regression equations from second-order polynomial fits in the form: $y = y_0 + ax + bx^2$

Run	Temp (°C)	pH	Surface area (m^2)	P_{O2} (atm)	Initial rate (mol/L s)	R_{sp} (mol /m^2 s)	k ($mol^{0.68}$ $L^{0.32}$ / m^2 s)
P036	19.5	3.15	0.119	0.995	3.7436×10^{-10}	5.5053×10^{-9}	2.9137×10^{-8}
P037	20.0	3.15	0.119	0.995	4.7612×10^{-10}	7.0018×10^{-9}	3.7057×10^{-8}
P054	34.0	3.09	0.033	0.995	6.7612×10^{-10}	3.5855×10^{-8}	1.9856×10^{-7}
P055	35.0	3.10	0.033	0.995	5.5955×10^{-10}	2.9673×10^{-8}	1.6552×10^{-7}
P060	21.0	2.97	0.033	0.995	2.0045×10^{-10}	1.0630×10^{-8}	5.4668×10^{-8}
P061	22.0	2.98	0.033	0.995	2.5028×10^{-10}	1.3272×10^{-8}	6.8707×10^{-8}
P065	13.0	2.96	0.033	0.995	1.4504×10^{-10}	7.6915×10^{-9}	3.8092×10^{-8}
P066	4.0	3.04	0.033	0.995	1.4125×10^{-10}	7.4905×10^{-9}	4.3234×10^{-8}
P067	4.0	3.08	0.033	0.995	1.1908×10^{-10}	6.3148×10^{-9}	3.8705×10^{-8}
P068	21.0	2.98	0.033	0.100	1.9472×10^{-10}	1.0326×10^{-8}	9.1946×10^{-8}
P069	22.5	3.00	0.033	0.100	1.6898×10^{-10}	8.9611×10^{-9}	8.0185×10^{-8}
P072	21.0	3.00	0.033	0.010	6.7875×10^{-11}	3.5994×10^{-9}	5.4997×10^{-8}
P073	23.0	3.50	0.033	0.010	4.6451×10^{-11}	2.4633×10^{-9}	4.1835×10^{-8}
P074	22.0	3.90	0.033	0.995	1.3862×10^{-10}	7.3511×10^{-9}	4.5230×10^{-8}
P075	22.0	1.97	0.033	0.995	1.5021×10^{-10}	7.9657×10^{-9}	3.3953×10^{-8}

Table 1. Run conditions, initial rates, specific rates, and rate constants

Run	Initial rate (mol/kg s)	Rsqr	Standard Error
P036	$3.7436 \times 10^{-10} \pm 2.6086 \times 10^{-11}$	0.9854	2.6086×10^{-11}
P037	$4.7612 \times 10^{-10} \pm 6.2465 \times 10^{-11}$	0.9749	6.2465×10^{-11}
P054	$6.7612 \times 10^{-10} \pm 2.6959 \times 10^{-11}$	0.9984	2.6959×10^{-11}
P055	$5.5955 \times 10^{-10} \pm 2.7492 \times 10^{-11}$	0.9981	2.7492×10^{-11}
P060	$2.0045 \times 10^{-10} \pm 1.7439 \times 10^{-11}$	0.9830	1.7439×10^{-11}
P061	$2.5028 \times 10^{-10} \pm 1.5913 \times 10^{-11}$	0.9924	1.5913×10^{-11}
P065	$1.4504 \times 10^{-10} \pm 1.3475 \times 10^{-11}$	0.9584	1.3475×10^{-11}
P066	$1.4125 \times 10^{-10} \pm 9.5231 \times 10^{-12}$	0.9860	9.5231×10^{-12}
P067	$1.1908 \times 10^{-10} \pm 7.3656 \times 10^{-12}$	0.9914	7.3656×10^{-12}
P068	$1.9472 \times 10^{-10} \pm 1.9240 \times 10^{-11}$	0.9774	1.9240×10^{-11}
P069	$1.6898 \times 10^{-10} \pm 1.8047 \times 10^{-11}$	0.9758	1.8047×10^{-11}
P072	$6.7875 \times 10^{-11} \pm 6.1367 \times 10^{-12}$	0.9680	6.1367×10^{-12}
P073	$4.6451 \times 10^{-11} \pm 9.8004 \times 10^{-12}$	0.9601	9.8004×10^{-12}
P074	$1.3862 \times 10^{-10} \pm 6.4879 \times 10^{-12}$	0.9974	6.4879×10^{-12}
P075	$1.5021 \times 10^{-10} \pm 3.3460 \times 10^{-11}$	0.9474	3.3460×10^{-11}

Table 2. Initial rates and standard error

2.2 Plots of Fe concentration in moles per kilogram versus time in seconds for each run

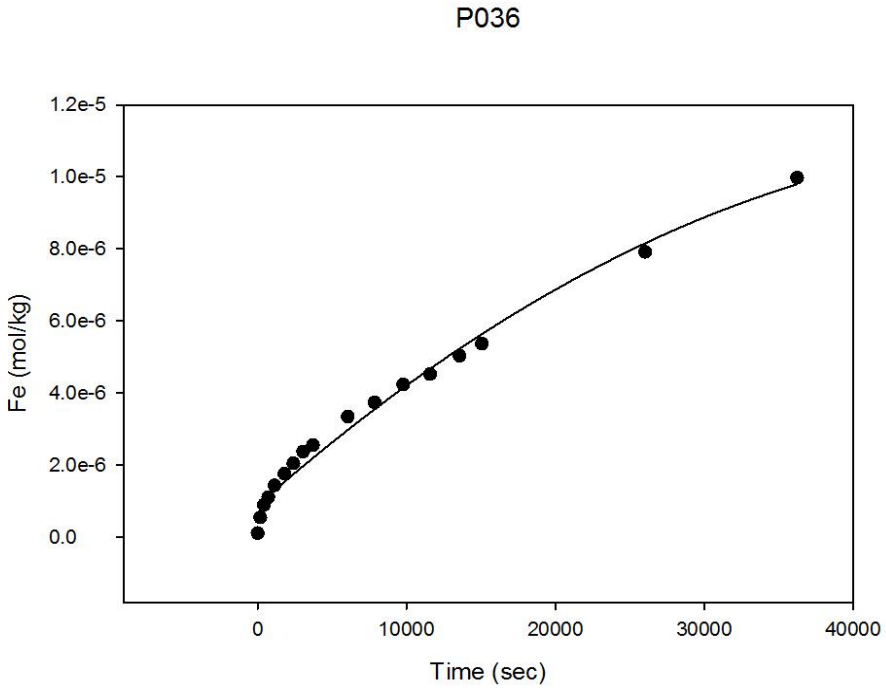

Fig. 5. P036 Fe (mol/kg) vs. Time (sec)

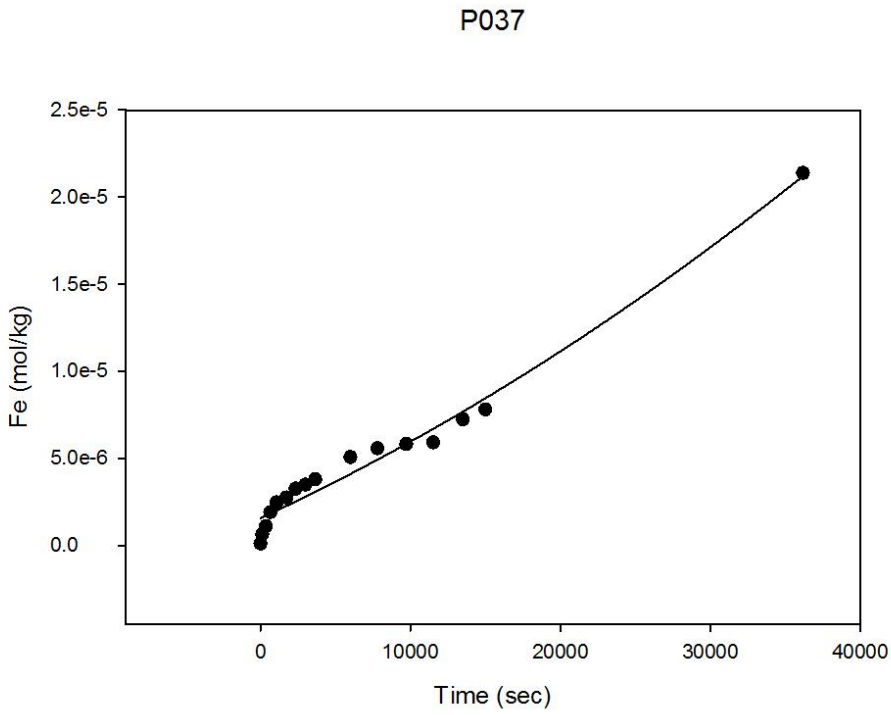

Fig. 6. P037 Fe (mol/kg) vs. Time (sec)

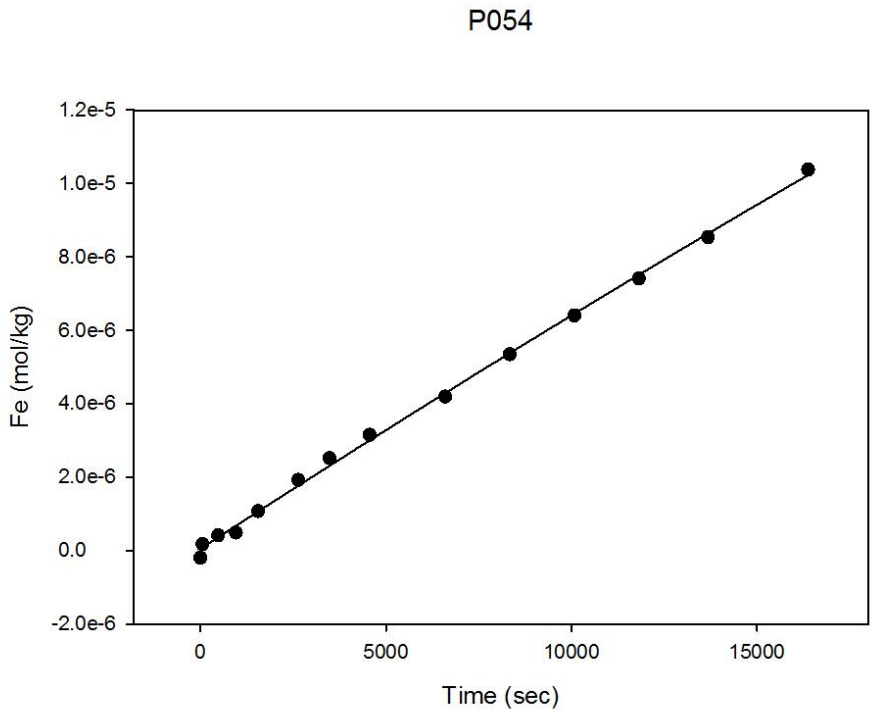

Fig. 7. P054 Fe (mol/kg) vs. Time (sec)

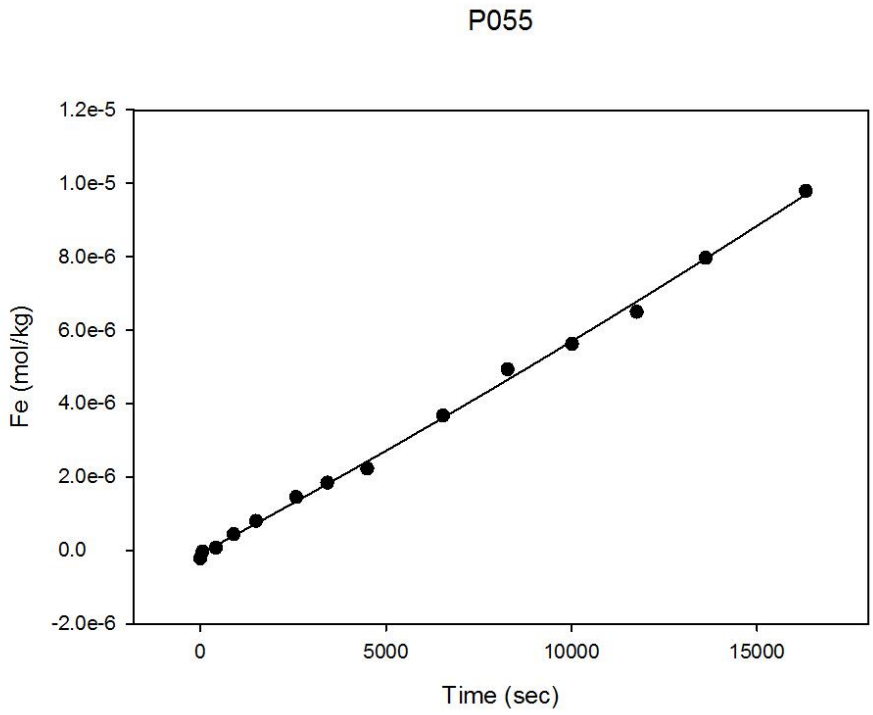

Fig. 8. P055 Fe (mol/kg) vs. Time (sec)

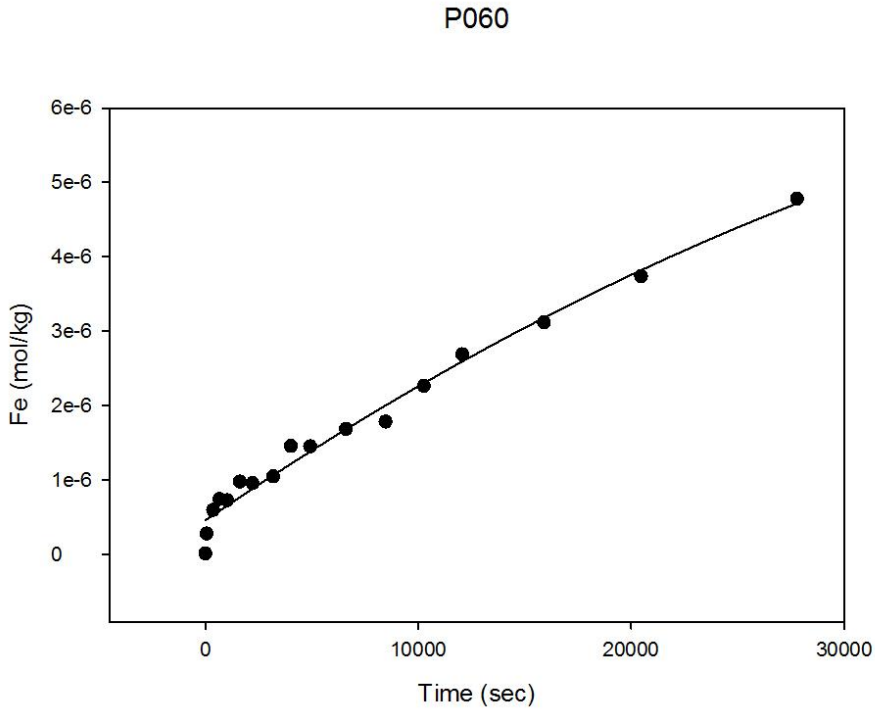

Fig. 9. P060 Fe (mol/kg) vs. Time (sec)

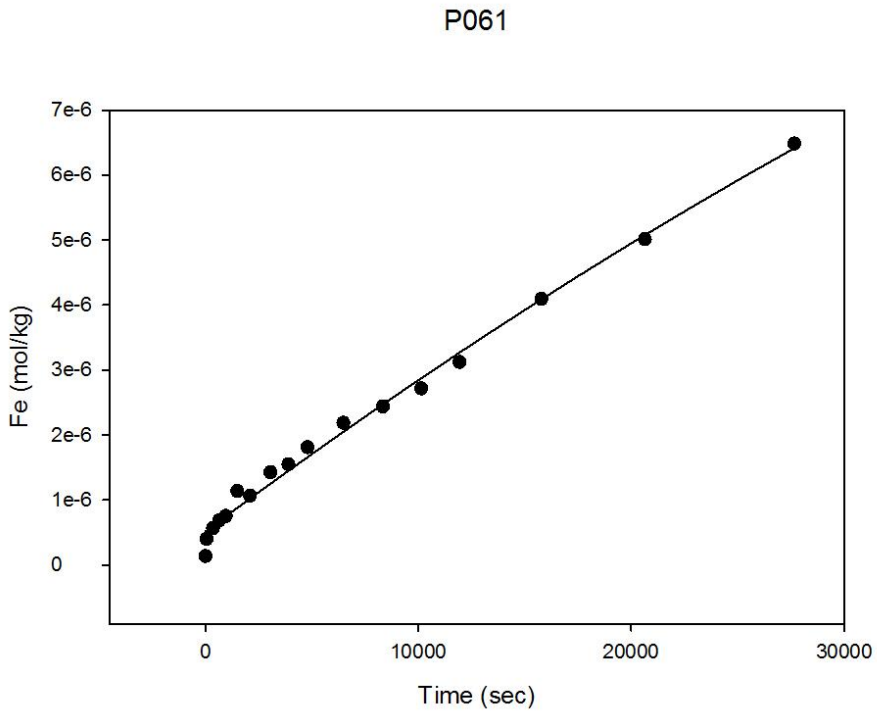

Fig. 10. P061 Fe (mol/kg) vs. Time (sec)

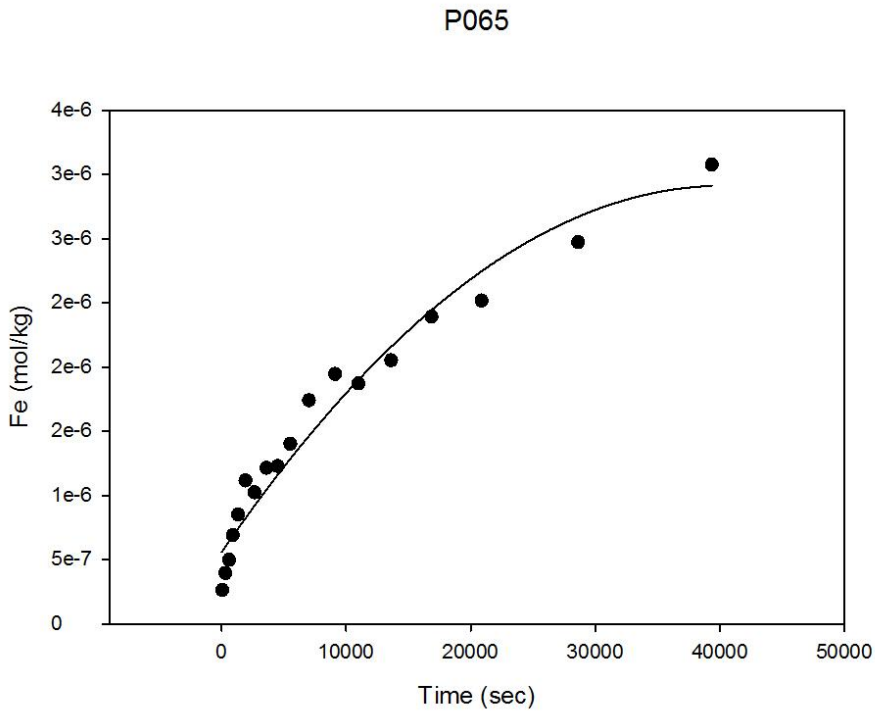

Fig. 11. P065 Fe (mol/kg) vs. Time (sec)

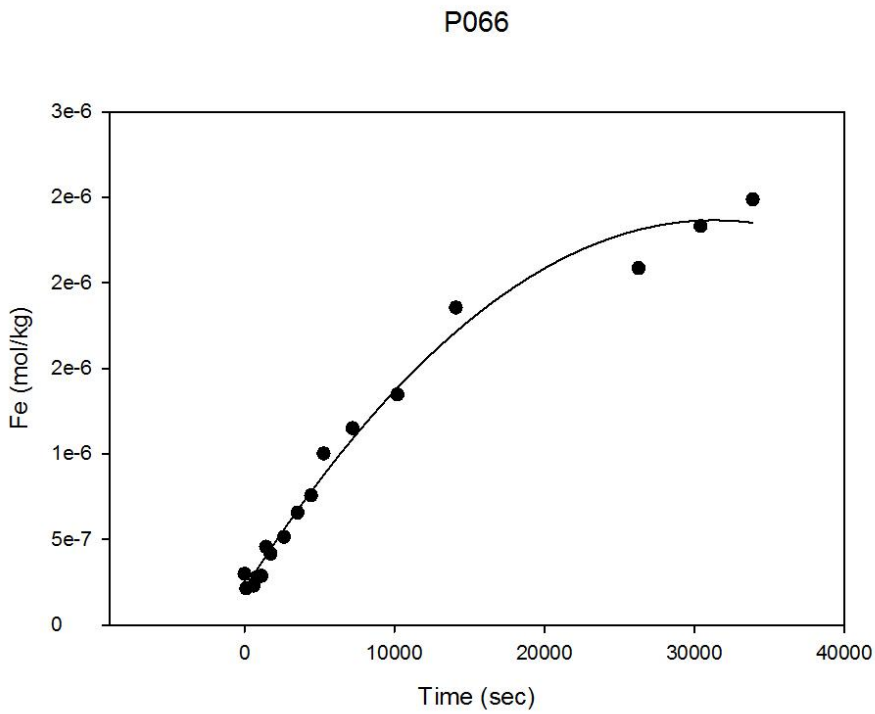

Fig. 12. P066 Fe (mol/kg) vs. Time (sec)

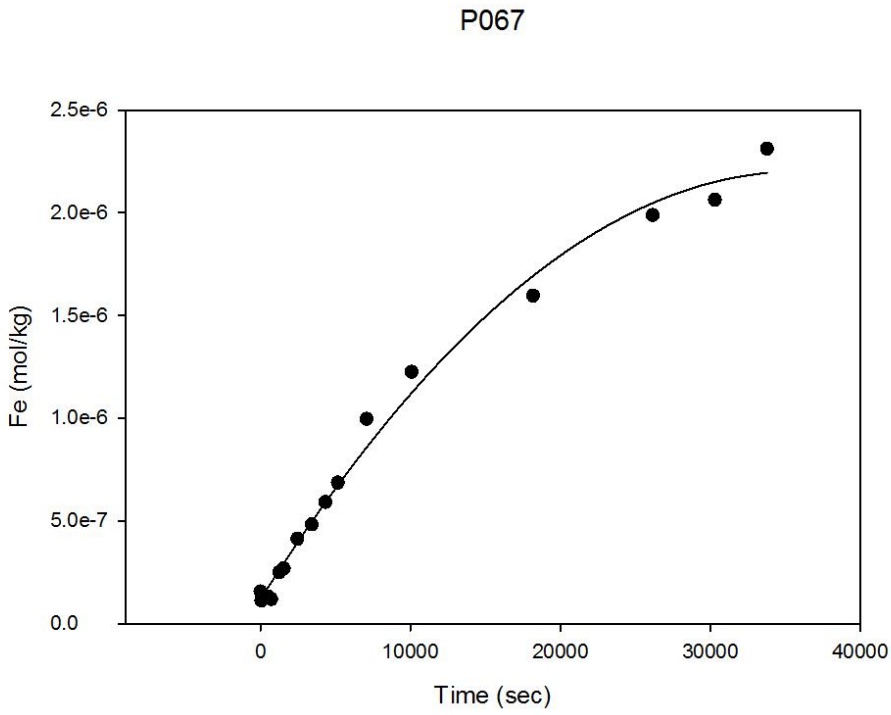

Fig. 13. P067 Fe (mol/kg) vs. Time (sec)

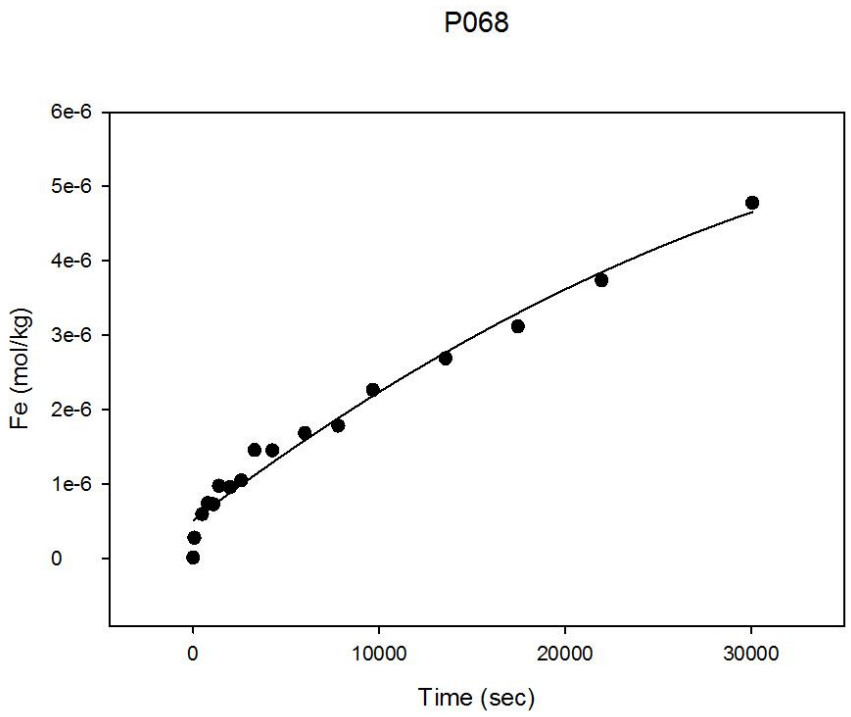

Fig. 14. P068 Fe (mol/kg) vs. Time (sec)

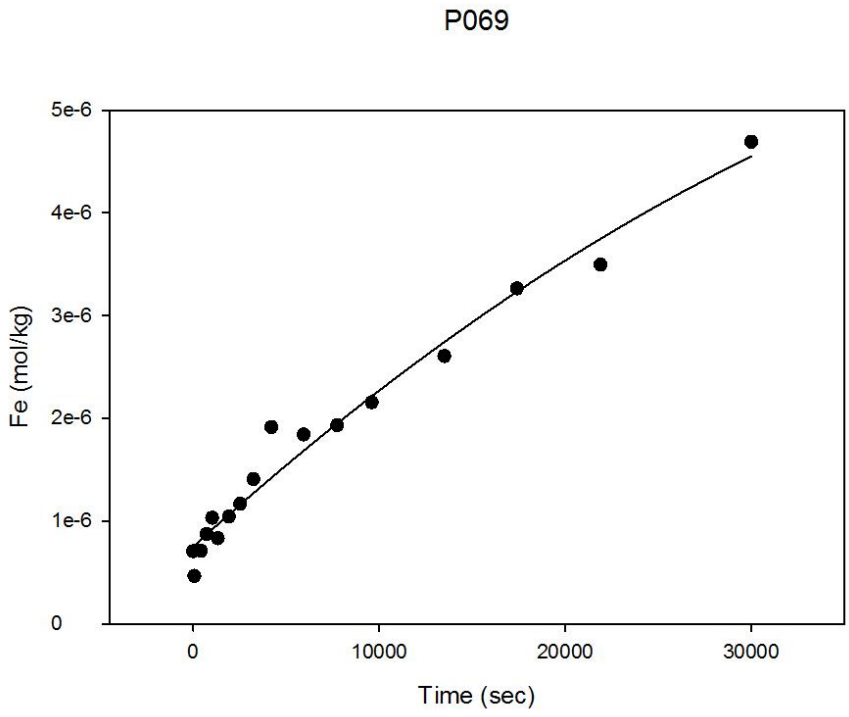

Fig. 15. P069 Fe (mol/kg) vs. Time (sec)

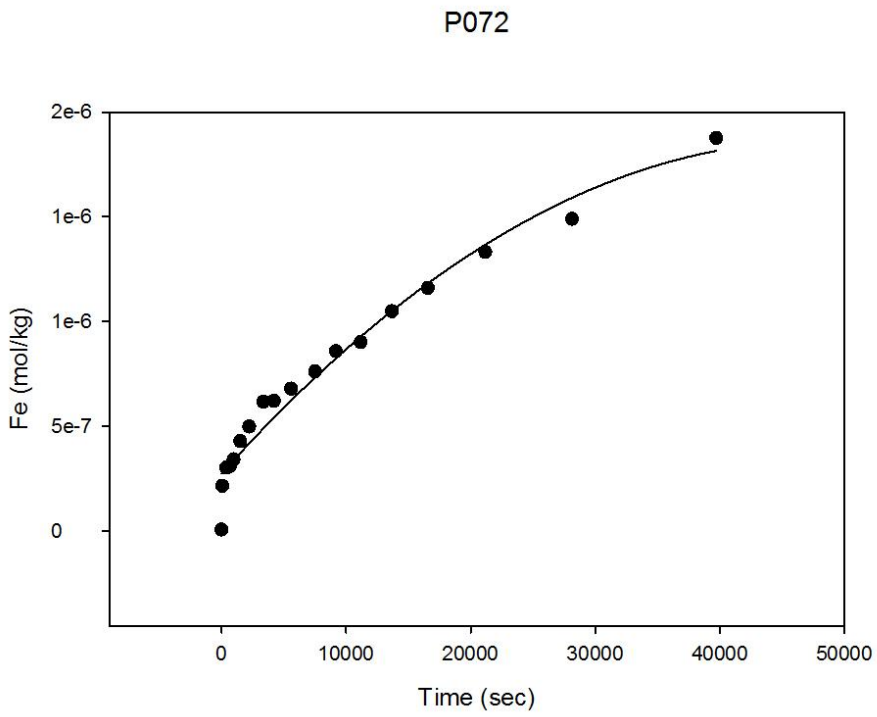

Fig. 16. P072 Fe (mol/kg) vs. Time (sec)

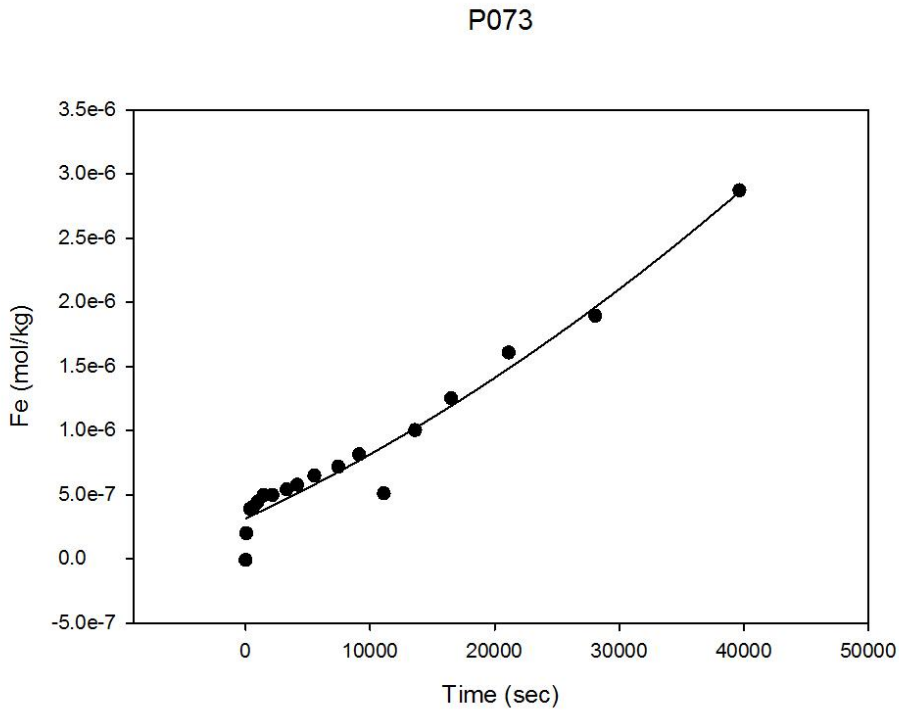

Fig. 17. P073 Fe (mol/kg) vs. Time (sec)

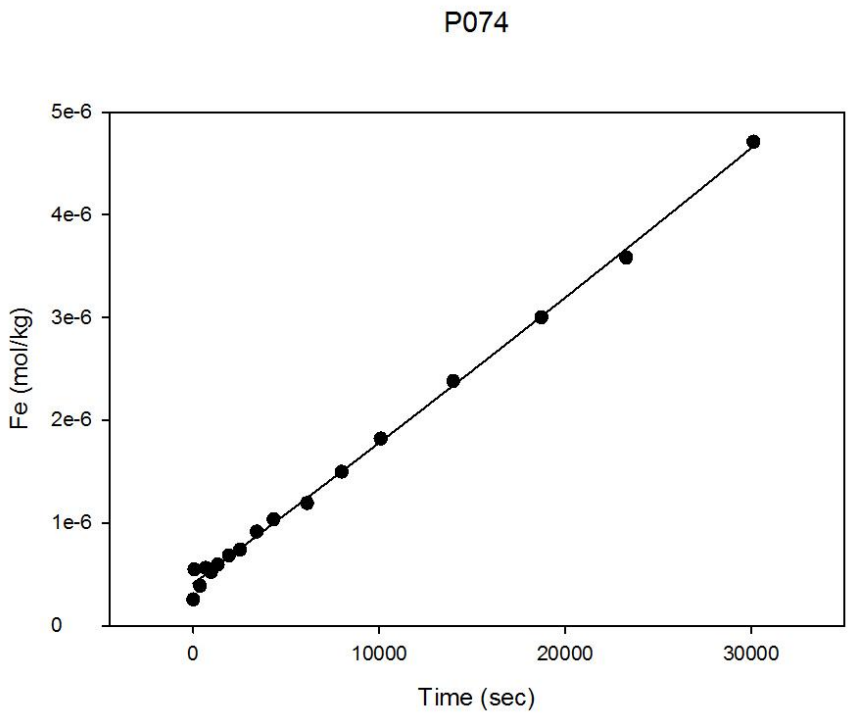

Fig. 18. P074 Fe (mol/kg) vs. Time (sec)

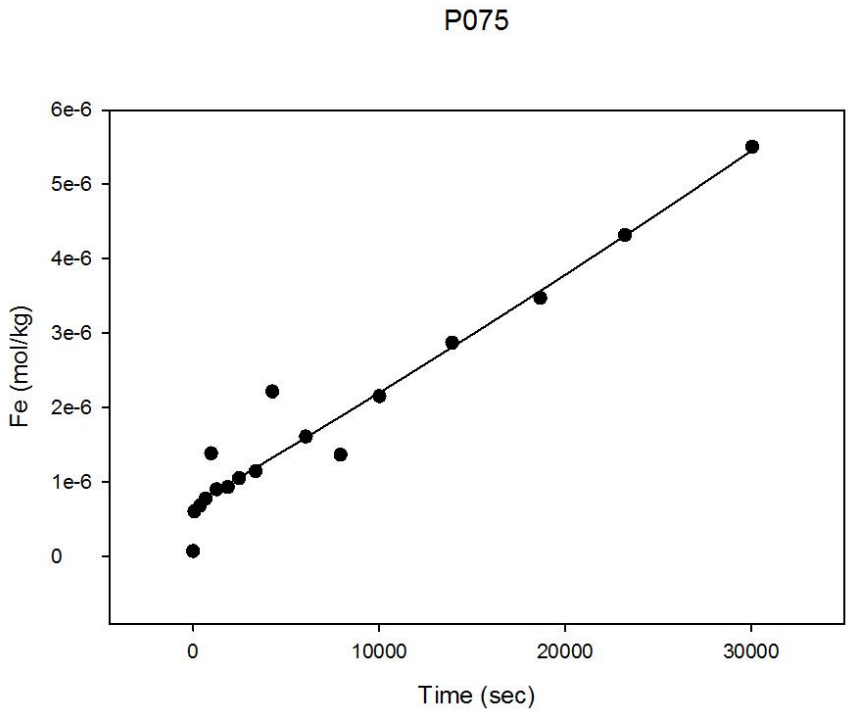

Fig. 19. P075 Fe (mol/kg) vs. Time (sec)

Raw data from runs incorporated into rate law. Samples were diluted 10 fold with 2% HNO_3. Samples labeled FD are duplicates. Fe [#1] was measured with helium and Fe [#2] with hydrogen. Fe [#1] concentrations were used in rate calculations.

Time (min)	Sample	Fe / 56 [#1]	Fe / 56 [#2]	Dilution factor	Undiluted [#1]	Undiluted [#2]	Fe (mol/kg)
0	P036-00	0.6555	0.589	9.987355176	6.546711318	5.882552198	1.11369E-07
3	P036-01	3.202	3.099	10.01795624	32.07749587	31.04564637	5.45682E-07
7	P036-02	5.287	5.194	9.93106113	52.50552019	51.58193151	8.93191E-07
12	P036-03	6.516	6.618	10.00651824	65.20247286	66.22313772	1.10918E-06
19	P036-04	8.367	8.41	10.08852633	84.41069983	84.84450646	1.43594E-06
30	P036-05	10.24	9.98	10.0851955	103.2724019	100.6502511	1.75681E-06
40	P036-06	11.67	11.44	10.31352286	120.3588118	117.9867015	2.04747E-06
51	P036-07	13.55	13.46	10.30407143	139.6201679	138.6928014	2.37513E-06
62	P036-08	14.64	14.88	10.24697039	150.0156466	152.4749195	2.55197E-06
101	P036-09	19.13	19.41	10.27443242	196.5498922	199.4267333	3.34358E-06
131	P036-10	21.32	21.95	10.30672217	219.7393168	226.2325517	3.73807E-06
163	P036-11	24.72	24.45	10.07111536	248.9579717	246.2387706	4.23512E-06
193	P036-12	26.68	26.75	9.962150968	265.7901878	266.4875384	4.52146E-06
FD	P036-13	25.29	24.61	9.573663348	242.1179461	235.607855	4.11876E-06
226	P036-14	29.01	28.28	10.19516162	295.7616385	288.3191706	5.03131E-06
251	P036-15	30.94	31.03	10.19738171	315.5069902	316.4247545	5.36721E-06
434	P036-16	46.31	45.62	10.0472297	465.2872074	458.3546189	7.91517E-06
FD	P036-17	44.9	43.98	9.920229706	445.4183138	436.2917025	7.57718E-06
604	P036-18	57.41	58.78	10.21087453	586.2063068	600.1952049	9.97217E-06

Table 3. Run P036 at 19.5°C, pH 3.15, 0.119 m^2, P_{O2} 0.995 atm

Time (min)	Sample	Fe / 56 [#1]	Fe / 56 [#2]	Dilution factor	Undiluted [#1]	Undiluted Fe [#2]	Fe (mol/kg)
0	P037-00	0.5738	0.5155	10.04030855	5.761129049	35.76357907	9.80047E-08
2	P037-01	3.573	3.562	10.14445308	36.24613087	65.1273888	6.16596E-07
6	P037-02	6.405	6.42	10.10664847	64.73308343	117.4392552	1.1012E-06
11	P037-03	11.29	11.62	9.903332998	111.8086295	134.9824288	1.90202E-06
18	P037-04	14.53	13.63	9.937717251	144.3950317	167.9474215	2.45636E-06
29	P037-05	16.22	16.9	9.903844195	160.6403528	183.2211176	2.73271E-06
39	P037-06	18.85	18.5	10.12918588	190.9351538	207.8508942	3.24807E-06
50	P037-07	20.52	20.52	9.96370768	204.4552816	221.792133	3.47806E-06
61	P037-08	22.13	22.26	10.06692326	222.7810117	274.9276741	3.78981E-06
100	P037-09	27.43	27.31	10.84439701	297.4618099	332.7061002	5.06023E-06
130	P037-10	31.09	30.68	10.52106453	327.0998962	356.9797194	5.56442E-06
162	P037-11	33.2	33.93	10.29582807	341.8214918	362.0013148	5.81485E-06
192	P037-12	34.84	35.16	9.96736963	347.2631579	359.8220436	5.90742E-06
FD	P037-13	35.4	36.1	10.11848749	358.1944571	424.2681804	6.09338E-06
225	P037-14	40.83	41.93	10.41055866	425.0631102	478.5733817	7.23091E-06
250	P037-15	43.33	45.97	10.58833065	458.792367	1250.48185	7.80469E-06
603	P037-17	119.1	118.1	10.55446823	1257.037166	777.2310404	2.13839E-05
FD	P037-18	72.49	73.64	10.04756364	728.3478882	-9.666760977	1.23902E-05

Table 4. Run P037 at 20.0°C, pH 3.15, 0.119 m^2, P_{O2} 0.995 atm

Time (min)	Sample	Fe / 56 [#1]	Fe / 56 [#2]	Dilution factor	Undiluted [#1]	Undiluted [#2]	Fe (mol/kg)
0	P054-00	-1.149	-0.9657	10.25898842	-11.7875777	-9.907105119	-2.00523E-07
1	P054-01	0.975	1.009	10.34825056	10.0895443	10.44138482	1.71637E-07
8	P054-02	2.352	2.731	10.20817428	24.0096259	27.87852395	4.08437E-07
16	P054-03	3.241	3.537	8.765778401	28.4098878	31.0045582	4.83291E-07
26	P054-04	6.09	6.458	10.32955568	62.90699411	66.7082706	1.07013E-06
44	P054-05	10.97	11.85	10.27915418	112.7623213	121.807977	1.91824E-06
58	P054-06	14.58	14.08	10.13121881	147.7131702	142.6475608	2.5128E-06
76	P054-07	17.77	17.45	10.41134926	185.0096764	181.6780446	3.14727E-06
110	P054-08	23.59	24.43	10.43739827	246.2182253	254.9856398	4.18851E-06
139	P054-09	30.65	31.58	10.24714598	314.0750243	323.6048701	5.34285E-06
168	P054-10	36.22	37.8	10.38893953	376.2873899	392.7019143	6.40116E-06
FD	P054-11	38.88	38.86	10.70653236	416.2699783	416.0558476	7.08132E-06
197	P054-12	43	43.82	10.13088611	435.6281029	443.9354295	7.41063E-06
228	P054-13	48.78	49.29	10.28273976	501.5920455	506.8362427	8.53277E-06
273	P054-14	59.01	59.36	10.33383746	609.7997483	613.4165914	1.03735E-05

Table 5. Run P054 at 34.0°C, pH 3.09, 0.033 m^2, P_{O2} 0.995 atm

Time (min)	Sample	Fe / 56 [#1]	Fe / 56 [#2]	Dilution factor	Undiluted [#1]	Undiluted [#2]	Fe (mol/kg)
0	P055-00	-1.276	-1.235	10.19465657	-13.00838178	-12.59040086	-2.2129E-07
1	P055-01	-0.2202	-0.02142	10.22411558	-2.25135025	-0.219000556	-3.82986E-08
7	P055-02	0.3746	0.6042	10.11513158	3.789128289	6.1115625	6.44583E-08
15	P055-03	2.447	2.729	10.40824097	25.46896566	28.40408961	4.33262E-07
25	P055-04	5.158	6.255	9.061849916	46.74102187	56.68187123	7.95129E-07
43	P055-05	8.127	8.544	10.46682847	85.06391498	89.42858245	1.44705E-06
57	P055-06	10.64	10.98	10.15822498	108.0835138	111.5373103	1.83865E-06
75	P055-07	12.9	13.9	10.12901399	130.6642805	140.7932945	2.22278E-06
109	P055-08	20.95	21.8	10.28535206	215.4781257	224.220675	3.66558E-06
138	P055-09	28.21	29.33	10.26943238	289.7006873	301.2024516	4.92821E-06
167	P055-10	32.45	34.33	10.18673328	330.5594948	349.7105534	5.62327E-06
FD	P055-11	33.02	34.51	10.3526712	341.8452031	357.2706832	5.81526E-06
196	P055-12	37.89	39.94	10.07805094	381.8573503	402.5173547	6.49592E-06
227	P055-13	46.44	47.47	10.08299345	468.2542156	478.6396989	7.96565E-06
272	P055-14	56.52	57.3	10.1849786	575.6549906	583.5992739	9.79268E-06

Table 6. Run P055 at 35.0^{o}C, pH 3.10, 0.033 m^{2}, P_{O2} 0.995 atm

Time (min)	Sample	Fe / 56 [#1]	Fe / 56 [#2]	Dilution factor	Undiluted [#1]	Undiluted [#2]	Fe (mol/kg)
0	P060-00	1.078	1.487	9.772679203	10.53494818	14.53197397	1.79214E-07
1	P060-01	2.115	2.382	10.25461341	21.68850736	24.42648914	3.68951E-07
6	P060-02	2.833	3.077	10.20059883	28.89829649	31.38724261	4.916E-07
11	P060-03	4.076	4.26	10.1791589	41.49025168	43.36321692	7.05806E-07
17	P060-04	4.883	5.18	10.15995888	49.61107919	52.62858698	8.43952E-07
27	P060-05	5.976	6.329	10.17497531	60.80565243	64.39741871	1.03439E-06
37	P060-06	6.435	6.601	10.30344504	66.3026688	68.01304068	1.1279E-06
53	P060-07	7.727	7.913	10.33316248	79.84434649	81.76631471	1.35826E-06
67	P060-08	8.787	9.117	10.35981917	91.03173108	94.45047141	1.54857E-06
82	P060-09	9.63	9.97	10.15729112	97.81471348	101.2681925	1.66396E-06
110	P060-10	12.54	12.08	10.17108822	127.5454463	122.8667457	2.16972E-06
141	P060-11	13.77	14.49	10.26642446	141.3686649	148.7604905	2.40487E-06
171	P060-12	15.85	16.56	10.26079391	162.6335835	169.9187472	2.76662E-06
201	P060-13	17.09	18.01	10.26784348	175.477445	184.923861	2.98511E-06
265	P060-14	22.97	23.22	10.19600338	234.2021977	236.7511986	3.9841E-06
341	P060-16	29.32	30.03	10.06823183	295.2005572	302.3490018	5.02177E-06
FD	P060-17	29.06	29.47	9.988228847	290.2579303	294.3531041	4.93769E-06
463	P060-18	37.96	39.11	10.37912875	393.9917274	405.9277254	6.70234E-06

Table 7. Run P060 at 21.0^{o}C, pH 2.97, 0.033 m^2, P_{O2} 0.995 atm

Time (min)	Sample	Fe / 56 [#1]	Fe / 56 [#2]	Dilution factor	Undiluted [#1]	Undiluted [#2]	Fe (mol/kg)
0	P065-00	1.314	1.125	12.25249873	16.09978333	13.78406107	2.73879E-07
1	P065-01	1.254	1	12.24078574	15.34994532	12.24078574	2.61124E-07
5	P065-02	1.87	1.587	12.39338449	23.17562899	19.66830118	3.94249E-07
10	P065-03	2.371	2.324	12.32519169	29.2230295	28.64374549	4.97124E-07
15	P065-04	3.28	3.142	12.34325702	40.48588302	38.78251355	6.8872E-07
22	P065-05	4.071	3.905	12.27056665	49.95347685	47.91656278	8.49777E-07
32	P065-06	5.223	5.165	12.5319352	65.45429753	64.72744529	1.11347E-06
44	P065-07	5.837	5.456	10.29967466	60.119201	56.19502496	1.02271E-06
60	P065-08	6.983	6.382	10.20482403	71.26028617	65.12718693	1.21224E-06
75	P065-09	6.974	7.033	10.34321974	72.13361445	72.74386442	1.22709E-06
92	P065-10	7.981	8.035	10.31367527	82.31344236	82.87038083	1.40026E-06
117	P065-11	9.954	9.951	10.26617502	102.1895061	102.1587076	1.73838E-06
152	P065-12	10.87	10.3	10.50854784	114.2279151	108.2380428	1.94317E-06
183	P065-13	10.65	10.81	10.32359986	109.9463385	111.5981145	1.87034E-06
227	P065-14	11.76	11.72	10.25160627	120.5588897	120.1488255	2.05087E-06
FD	P065-15	12.49	12.26	10.28148391	128.415734	126.0509927	2.18453E-06
281	P065-16	13.68	13.24	10.27052088	140.5007257	135.9816965	2.39011E-06
348	P065-17	14.27	14.21	10.36460885	147.9029683	147.2810918	2.51603E-06
477	P065-18	17.07	16.83	10.22627394	174.5624962	172.1081904	2.96955E-06
656	P065-19	20.51	20.28	10.24402567	210.1049664	207.7488405	3.57417E-06

Table 8. Run P065 at 13.0^{o}C, pH 2.96, 0.033 m^{2}, P_{O2} 0.995 atm

Time (min)	Sample	Fe / 56 [#1]	Fe / 56 [#2]	Dilution factor	Undiluted [#1]	Undiluted [#2]	Fe (mol/kg)
0	P066-00	1.521	2.361	10.35798543	15.75449585	24.45520361	2.96959E-07
2	P066-01	1.079	0.7862	10.41434629	11.23707965	8.187759056	2.1181E-07
10	P066-02	1.2	1.044	10.08568205	12.10281846	10.52945206	2.28128E-07
14	P066-03	1.439	1.041	10.2852791	14.80051663	10.70697555	2.78977E-07
19	P066-04	1.468	1.33	10.31507762	15.14253394	13.71905323	2.85424E-07
24	P066-05	2.374	2.129	10.18167319	24.17129216	21.67678223	4.55609E-07
29	P066-06	2.136	1.936	10.31434485	22.0314406	19.96857163	4.15274E-07
44	P066-07	2.645	2.464	10.29807238	27.23840145	25.37445035	5.13421E-07
59	P066-08	3.359	3.16	10.34514619	34.74934605	32.69066196	6.54996E-07
74	P066-09	3.899	3.717	10.28269807	40.09223976	38.22078871	7.55705E-07
88	P066-10	5.123	4.962	10.36463613	53.0980309	51.42932449	1.00085E-06
120	P066-11	5.853	6.11	10.41176591	60.94006587	63.6158897	1.14867E-06
170	P066-12	6.911	6.854	10.33042196	71.39354617	70.80471212	1.34571E-06
235	P066-13	9.449	10.18	10.40679628	98.333818	105.9411861	1.85351E-06
FD	P066-14	9.287	9.374	10.09837668	93.78362425	94.66218303	1.76774E-06
438	P066-15	10.81	11.03	10.22662428	110.5498084	112.7996658	2.08377E-06
507	P066-16	11.88	12.12	10.40393425	123.5987389	126.0956831	2.32973E-06
565	P066-17	12.7	13.4	10.38236747	131.8560668	139.1237241	2.48538E-06

Table 9. Run P066 at 4.0^{o}C, pH 3.04, 0.033 m^{2}, P_{O2} 0.995 atm

Time (min)	Sample	Fe / 56 [#1]	Fe / 56 [#2]	Dilution factor	Undiluted [#1]	Undiluted [#2]	Fe (mol/kg)
0	P067-00	0.8865	0.5176	10.29762511	9.128844664	5.330050759	1.55294E-07
1	P067-01	0.6385	0.3417	10.27617213	6.561335902	3.511368015	1.11617E-07
8	P067-02	0.7834	0.3048	9.809502511	7.684764267	2.989936365	1.30728E-07
12	P067-03	0.7067	0.4871	9.834738344	6.950209588	4.790501047	1.18233E-07
16	P067-04	3.162	3.027	10.0227559	31.69195416	30.33888212	5.39124E-07
21	P067-05	1.465	1.158	9.984640569	14.62749843	11.56221378	2.48834E-07
26	P067-06	1.588	1.319	9.899822624	15.72091833	13.05786604	2.67434E-07
41	P067-07	2.414	2.114	10.03092522	24.21465349	21.20537592	4.11924E-07
57	P067-08	2.886	2.603	9.820126398	28.34088478	25.56178901	4.82117E-07
72	P067-09	3.543	3.32	9.803441058	34.73359167	32.54742431	5.90866E-07
86	P067-10	4.018	3.826	10.03203114	40.30870112	38.38255114	6.85706E-07
118	P067-11	5.698	5.63	10.26863397	58.51067637	57.81240926	9.95347E-07
168	P067-12	7.105	7.23	10.13020168	71.97508297	73.24135818	1.22439E-06
303	P067-13	9.26	9.398	10.12707284	93.77669447	95.17423053	1.59527E-06
FD	P067-14	8.966	8.94	9.888207864	88.65767171	88.40057831	1.50819E-06
436	P067-15	11.63	11.49	10.04578262	116.8324519	115.4260423	1.98748E-06
505	P067-16	12.04	12.55	10.06981086	121.2405228	126.3761263	2.06247E-06
563	P067-17	13.08	13.6	10.38729858	135.8658655	141.2672607	2.31126E-06

Table 10. Run P067 at 4.0^{o}C, pH 3.08, 0.033 m^2, P_{O2} 0.995 atm

Time (min)	Sample	Fe / 56 [#1]	Fe / 56 [#2]	Dilution factor	Undiluted [#1]	Undiluted [#2]	Fe (mol/kg)
0	P068-00	0.07679	0.1128	10.3589175	0.795461275	1.168485894	1.35319E-08
1	P068-01	1.578	1.52	10.42771078	16.45492761	15.85012039	2.79921E-07
8	P068-02	3.406	3.627	10.31810601	35.14346906	37.42377049	5.97839E-07
13	P068-03	4.231	4.096	10.31698932	43.6511818	42.25838825	7.42566E-07
18	P068-04	4.179	3.902	10.27370777	42.93382479	40.08800773	7.30363E-07
23	P068-05	5.603	5.247	10.26112126	57.49306243	53.84010326	9.78036E-07
33	P068-06	5.545	5.34	10.16658676	56.37372357	54.28957328	9.58994E-07
43	P068-07	6.065	6.012	10.17085899	61.68625979	61.14720426	1.04937E-06
55	P068-08	8.457	8.253	10.1208719	85.59221362	83.52755576	1.45604E-06
71	P068-09	8.256	8.735	10.34384042	85.39874651	90.35344607	1.45275E-06
100	P068-10	9.65	10.1	10.26652398	99.07195638	103.6918922	1.68535E-06
130	P068-11	10.38	11.17	10.10134759	104.851988	112.8320526	1.78368E-06
161	P068-12	12.88	13.13	10.33558825	133.1223766	135.7062737	2.26459E-06
226	P068-13	15.24	15.66	10.37204749	158.0700037	162.4262636	2.68899E-06
291	P068-14	17.97	18.77	10.204847	183.3811006	191.5449782	3.11956E-06
FD	P068-15	17.8	18.74	10.16038988	180.8549399	190.4057064	3.07659E-06
366	P068-16	21.33	22.43	10.30207002	219.7431536	231.0754306	3.73813E-06
501	P068-17	27.03	29.59	10.39251576	280.909701	307.5145414	4.77866E-06

Table 11. Run P068 at 21.0^{o}C, pH 2.98, 0.033 m^{2}, P_{O2} 0.100 atm

Time (min)	Sample	Fe / 56 [#1]	Fe / 56 [#2]	Dilution factor	Undiluted [#1]	Undiluted [#2]	Fe (mol/kg)
0	P069-00	4.011	3.392	10.30467052	41.33203346	34.95344241	7.03115E-07
1	P069-01	2.633	2.589	10.34557036	27.23988676	26.78468166	4.63388E-07
7	P069-02	4.018	3.986	10.35147965	41.59224523	41.26099788	7.07541E-07
12	P069-03	4.67	4.599	10.96025849	51.18440714	50.40622879	8.70717E-07
17	P069-04	5.991	6.073	10.09514009	60.47998426	61.30778575	1.02885E-06
22	P069-05	4.75	4.941	10.26277506	48.74818153	50.70837157	8.29273E-07
32	P069-06	6.014	6.151	10.17659932	61.2020683	62.59626241	1.04113E-06
42	P069-07	6.745	6.985	10.15564598	68.49983215	70.93718718	1.16528E-06
54	P069-08	8.154	8.478	10.14240844	82.70119843	85.98733876	1.40686E-06
70	P069-09	10.92	10.91	10.28968571	112.363368	112.2604711	1.91145E-06
99	P069-10	10.68	10.75	10.13493649	108.2411217	108.9505672	1.84133E-06
129	P069-11	11.11	11.32	10.21305411	113.4670312	115.6117726	1.93023E-06
160	P069-12	12.4	12.64	10.2092238	126.5943751	129.0445888	2.15354E-06
225	P069-13	14.93	15.59	10.25253089	153.0702862	159.8369566	2.60394E-06
290	P069-14	18.57	20.32	10.32598147	191.7534759	209.8239434	3.26199E-06
FD	P069-15	18.02	18.17	10.03760718	180.8776814	182.3833225	3.07698E-06
365	P069-16	20.14	21.01	10.1959192	205.3458126	214.2162623	3.49321E-06
500	P069-17	27.11	27.98	10.16859799	275.6706915	284.5173718	4.68954E-06

Table 12. Run P069 at 22.5^{o}C, pH 3.00, 0.033 m^{2}, P_{O2} 0.100 atm

Time (min)	Sample	Fe / 56 [#1]	Fe / 56 [#2]	Dilution factor	Undiluted [#1]	Undiluted [#2]	Fe (mol/kg)
0	P072-00	0.04345	0.398	10.22326317	0.444200785	4.068858742	7.55646E-09
1	P072-01	1.281	1.317	9.929751282	12.72001139	13.07748244	2.16385E-07
6	P072-02	1.767	1.866	10.07377437	17.80035931	18.79766297	3.02809E-07
11	P072-03	1.79	1.905	10.18111374	18.2241936	19.39502168	3.10019E-07
16	P072-04	2.003	1.934	10.05129037	20.13273461	19.43919557	3.42485E-07
25	P072-05	2.502	2.791	10.09070756	25.24695031	28.1631648	4.29485E-07
37	P072-06	2.909	2.928	10.07508879	29.30843328	29.49985997	4.98577E-07
56	P072-07	3.605	3.596	10.06835977	36.29643698	36.20582174	6.17452E-07
70	P072-08	3.641	3.746	10.02750587	36.51014886	37.56303697	6.21088E-07
93	P072-09	3.953	4.05	10.10431978	39.94237608	40.9224951	6.79475E-07
125	P072-10	4.405	4.538	10.16746411	44.78767943	46.13995215	7.619E-07
153	P072-11	4.984	5.184	10.12761115	50.47601398	52.50153621	8.58666E-07
186	P072-12	5.196	5.411	10.20642552	53.03258698	55.22696846	9.02157E-07
228	P072-13	6.016	6.093	10.25267099	61.68006868	62.46952434	1.04926E-06
276	P072-14	6.62	6.824	10.30570827	68.22378873	70.32615321	1.16058E-06
353	P072-15	7.787	7.467	10.04876193	78.24970913	75.03410531	1.33113E-06
FD	P072-16	7.856	8.345	10.13019043	79.58277605	84.53643917	1.35381E-06
469	P072-17	8.819	9.205	9.927890017	87.55406206	91.38622761	1.48941E-06
662	P072-18	10.89	10.86	10.12411509	110.2516133	109.9478898	1.87553E-06

Table 13. Run P072 at 21.0^{o}C, pH 3.00, 0.033 m^{2}, P_{O2} 0.010 atm

Time (min)	Sample	Fe / 56 [#1]	Fe / 56 [#2]	Dilution factor	Undiluted [#1]	Undiluted [#2]	Fe (mol/kg)
0	P073-00	-0.06533	-0.1252	10.13159885	-0.661897353	-1.268476176	-1.12598E-08
1	P073-01	1.13	0.9624	10.26197521	11.59603198	9.876124937	1.97264E-07
6	P073-02	2.268	2.219	10.02719855	22.74168631	22.25035358	3.86867E-07
11	P073-03	2.403	2.485	9.945247285	23.89842923	24.7139395	4.06545E-07
16	P073-04	2.585	2.704	10.05393028	25.98940978	27.18582748	4.42115E-07
24	P073-05	2.902	2.846	10.01991247	29.07778598	28.51667088	4.94653E-07
36	P073-06	2.867	3.328	10.14563009	29.08752146	33.76465693	4.94819E-07
55	P073-07	3.128	3.396	10.13534686	31.70336497	34.41963793	5.39318E-07
69	P073-08	3.393	3.586	9.960549313	33.79614382	35.71852984	5.74919E-07
92	P073-09	3.737	3.858	10.17847212	38.0369503	39.26854543	6.47061E-07
124	P073-10	4.194	4.313	10.04578156	42.13200785	43.32745585	7.16723E-07
152	P073-11	4.752	4.822	10.05425722	47.77783032	48.48162832	8.12766E-07
185	P073-12	3.926	4.072	7.614315113	29.89380113	31.00549114	5.08535E-07
227	P073-13	5.893	6.328	9.990830443	58.8759638	63.22197504	1.00156E-06
275	P073-14	7.351	7.783	9.987996399	73.42176153	77.73657597	1.249E-06
352	P073-15	9.367	9.249	10.07342055	94.35773031	93.16906668	1.60515E-06
FD	P073-16	8.467	9.518	9.893681321	83.76979975	94.16805882	1.42504E-06
468	P073-17	11.37	12.51	9.785459813	111.2606781	122.4161023	1.8927E-06
661	P073-18	16.62	17.85	10.15391171	168.7580126	181.247324	2.87081E-06

Table 14. Run P073 at 23.0^{o}C, pH 3.50, 0.033 m^{2}, P_{O2} 0.010 atm

Time (min)	Sample	Fe / 56 [#1]	Fe / 56 [#2]	Dilution factor	Undiluted [#1]	Undiluted [#2]	Fe (mol/kg)
0	P074-00	1.442	1.267	10.34426196	14.91642574	13.1061799	2.53749E-07
1	P074-01	3.078	2.665	10.42078393	32.07517292	27.77138916	5.45643E-07
6	P074-02	2.301	2.191	9.885184812	22.74581025	21.65843992	3.86937E-07
11	P074-03	3.185	3.154	10.33013187	32.90147	32.58123591	5.59699E-07
16	P074-04	3.02	2.899	10.12832868	30.58755262	29.36202485	5.20336E-07
22	P074-05	3.418	3.247	10.18212173	34.80249208	33.06134927	5.92038E-07
32	P074-06	3.911	3.83	10.25517721	40.10799808	39.27732872	6.82292E-07
42	P074-07	4.268	4.363	10.17994911	43.44802278	44.41511795	7.3911E-07
57	P074-08	5.271	5.128	10.191031	53.71692439	52.25960696	9.13799E-07
72	P074-09	5.912	5.897	10.27117041	60.72315947	60.56909192	1.03298E-06
102	P074-10	6.96	7.109	10.05843413	70.00670154	71.50540822	1.19091E-06
133	P074-11	8.712	8.649	10.10144002	88.00374548	87.36735476	1.49706E-06
FD	P074-12	8.703	8.805	10.25847812	89.27953511	90.32589988	1.51877E-06
168	P074-13	10.47	10.46	10.21109575	106.9101725	106.8080615	1.81869E-06
233	P074-14	13.71	13.55	10.20000815	139.8421117	138.2101104	2.37891E-06
312	P074-15	17.2	17.7	10.25454097	176.3781048	181.5053752	3.00043E-06
388	P074-16	21.01	21.01	10.01922104	210.5038341	210.5038341	3.58096E-06
502	P074-17	26.4	27.14	10.48657113	276.8454779	284.6055405	4.70952E-06

Table 15. Run P074 at 22.0^{o}C, pH 3.90, 0.033 m^{2}, P_{O2} 0.995 atm

Time (min)	Sample	Fe / 56 [#1]	Fe / 56 [#2]	Dilution factor	Undiluted [#1]	Undiluted [#2]	Fe (mol/kg)
0	P075-00	0.3987	0.2256	10.44718108	4.165291097	2.356884052	7.08573E-08
1	P075-01	3.499	3.453	10.17508553	35.60262427	35.13457034	6.05649E-07
6	P075-02	3.963	4.069	10.1082085	40.0588303	41.1303004	6.81456E-07
11	P075-03	4.469	4.324	10.1784299	45.48740321	44.01153088	7.73803E-07
16	P075-04	7.9	7.66	10.31413294	81.48165026	79.00625835	1.38611E-06
21	P075-05	5.213	4.986	10.15004683	52.9121941	50.60813347	9.00109E-07
31	P075-06	5.367	5.452	10.19952033	54.74082564	55.60778487	9.31216E-07
41	P075-07	6.043	6.03	10.22672016	61.8000699	61.66712254	1.0513E-06
56	P075-08	6.56	6.708	10.25905994	67.29943318	68.81777405	1.14486E-06
71	P075-09	12.39	12.6	10.51616609	130.2952979	132.5036928	2.2165E-06
101	P075-10	9.062	9.254	10.44156809	94.62149006	96.62627113	1.60964E-06
132	P075-11	9.194	9.169	8.722658684	80.19612394	79.97805748	1.36425E-06
FD	P075-12	10.56	10.8	10.23379005	108.0688229	110.5249325	1.8384E-06
167	P075-13	12.34	12.55	10.25179307	126.5071265	128.6600031	2.15206E-06
232	P075-14	16.7	17	10.11108638	168.8551426	171.8884685	2.87246E-06
311	P075-15	20.26	20.99	10.07213088	204.0613717	211.4140272	3.47136E-06
387	P075-16	25.1	26.27	10.11168004	253.803169	265.6338346	4.31754E-06
501	P075-17	31.9	33.17	10.14436998	323.6054022	336.4887521	5.50497E-06

Table 16. Run P075 at 22.0^{o}C, pH 1.97, 0.033 m^{2}, P_{O2} 0.995 atm

Temp (°C)	Benson & Krause 1984 C*$_o$ (mg/L)	Calculated C*$_o$ (mg/L)		
		P_{O2} = 0.010	P_{O2} = 0.100	P_{O2} = 0.995
2.0	10.875	0.519	5.192	51.660
4.0	10.352	0.494	4.942	49.175
5.0	10.107	0.483	4.825	48.011
8.0	9.431	0.450	4.503	44.800
10.0	9.223	0.440	4.403	43.812
13.0	8.471	0.404	4.044	40.240
19.0	7.533	0.360	3.596	35.784
20.0	7.396	0.353	3.531	35.133
21.0	7.262	0.347	3.467	34.497
22.0	7.134	0.341	3.406	33.889
23.0	7.009	0.335	3.467	34.497
30.0	6.236	0.298	2.977	29.623
34.0	5.858	0.280	2.797	27.827

Table 17. C*$_o$ in mg O_2 per liter seawater and C†$_o$ in mol O_2 per kilogram seawater calculated using Benson and Krause (1984)

Benson & Krause 1984 $C\dagger_o$ (µmol/kg) Using 1.028 kg/dm3 for ρs	Calculated $C\dagger_o$ (mol/kg) Using 1.025 kg/dm³ for ρs			Calculated $C\dagger_o$ (mol/kg) Using 1.050 kg/dm³ for ρs		
	P_{O2} = 0.010	P_{O2} = 0.100	P_{O2} = 0.995	P_{O2} = 0.010	P_{O2} = 0.100	P_{O2} = 0.995
330.6	0.000158	0.001583	0.015750	0.000155	0.001545	0.015375
314.77	0.000151	0.001507	0.014993	0.000147	0.001471	0.014636
307.36	0.000147	0.001471	0.014638	0.000144	0.001436	0.014290
286.91	0.000137	0.001373	0.013659	0.000134	0.001340	0.013334
274.61	0.000134	0.001342	0.013358	0.000131	0.001311	0.013040
257.91	0.000123	0.001233	0.012269	0.000120	0.001204	0.011977
229.68	0.000110	0.001097	0.010910	0.000107	0.001070	0.010650
225.54	0.000108	0.001077	0.010712	0.000105	0.001051	0.010457
221.53	0.000106	0.001057	0.010518	0.000103	0.001032	0.010267
217.67	0.000104	0.001038	0.010332	0.000101	0.001014	0.010086
213.92	0.000102	0.001020	0.010151	0.000100	0.000996	0.009910
190.74	0.000091	0.000908	0.009032	0.000089	0.000886	0.008817
179.41	8.52689E-05	0.0008527	0.00848426	8.3239E-05	0.0008324	0.0082823

Table 18. $C\dagger_o$ (µmol/kg) from Benson & Krause (1984) and $C\dagger_o$ (mol/kg) calculated using 1.025 and 1.050 kg/dm³ as the density of seawater

4. APPENDIX D: Flow-Through Experiments

Due to time constraints a full flow-through study was not completed. Four preliminary experiments were run. A 1 L Teflon © vessel was used instead of a 2 L vessel so less water would be required. Additional glass tubes were added to accommodate influent and effluent flow as well as mixing within the vessel. The sample was contained within two pieces of nylon mesh within the sample platform to avoid abrasion (Rimstidt & Dove, 1986) as in batch setup. The setup is shown in Fig. 1. Experiments were run for approximately 4 hours.

Fig. 20. Flow-through setup with influent above bath and effluent below/adjacent. Peristaltic pumps pump seawater in and out at equal rates so that solution volume remains constant. Seawater flows 13 mL/min, and a third pump mixes solution inside the vessel.

Two runs were conducted at pH 7.5 which produced erratic or non-detect amounts of Fe in solution. For convenience these were ran at 20.0°C and P_{O2} = 0.995 atm with grains 105-160 µm (Figs. 21 and 22). Two runs conducted at pH 3.0 showed more promising, yet inconsistent results (Figs. 23 and 24).

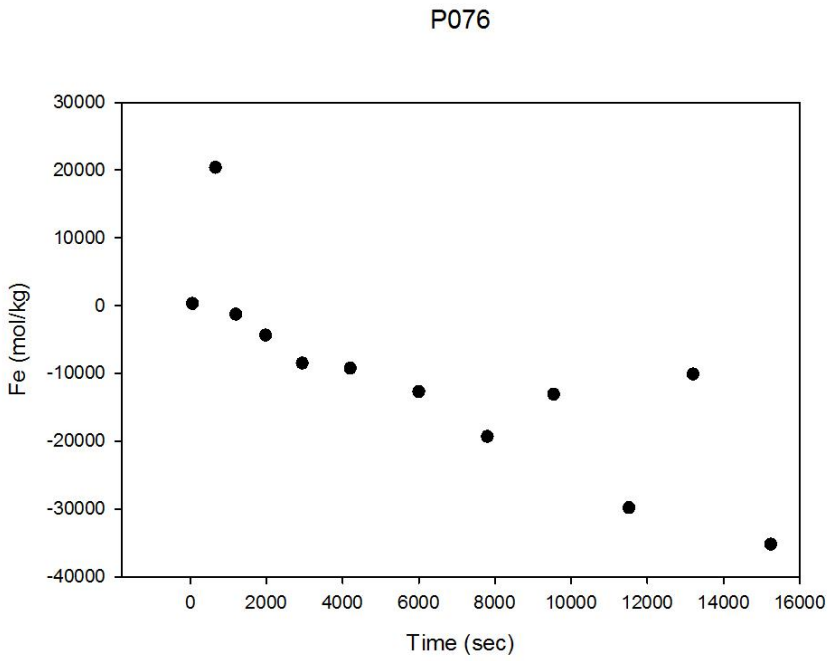

Fig. 21. First attempt flow-through run data. Values below 0 should be considered "non-detect."

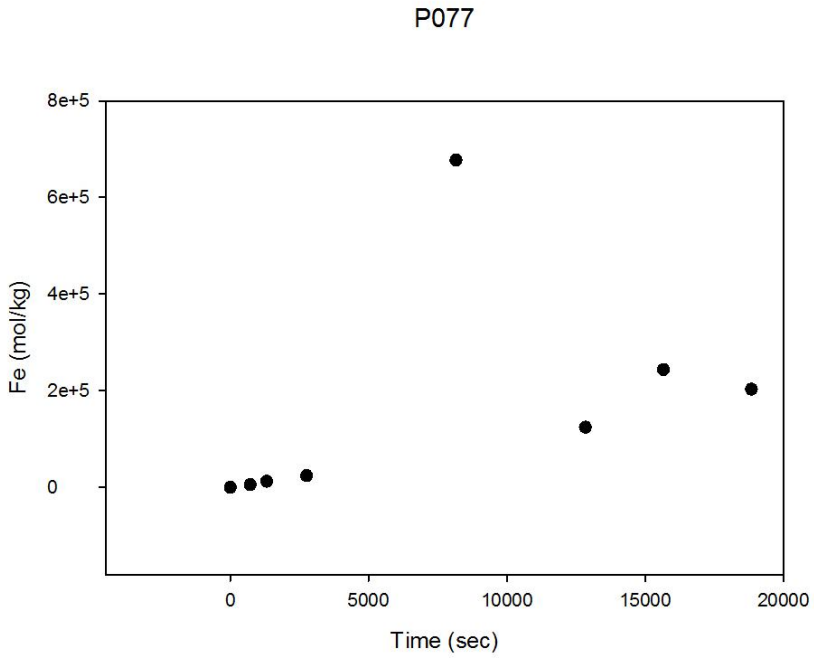

Fig. 22. Second flow-through run at pH 7.5, showing measurable yet erratic concentrations of Fe.

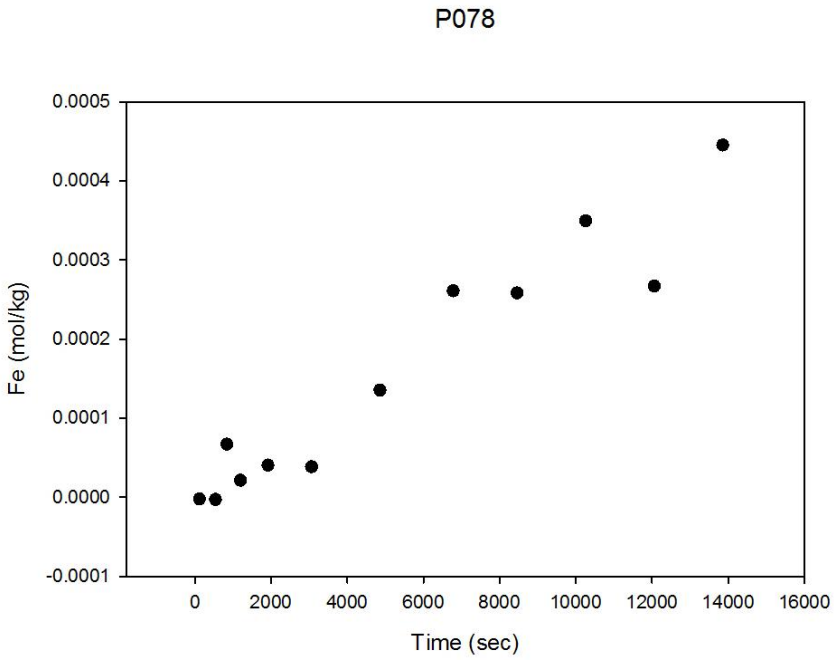

Fig. 23. Flow-through run at pH 3.0, 20.0^{o}C P_{O2} = 0.995 atm, and 105-160 µm

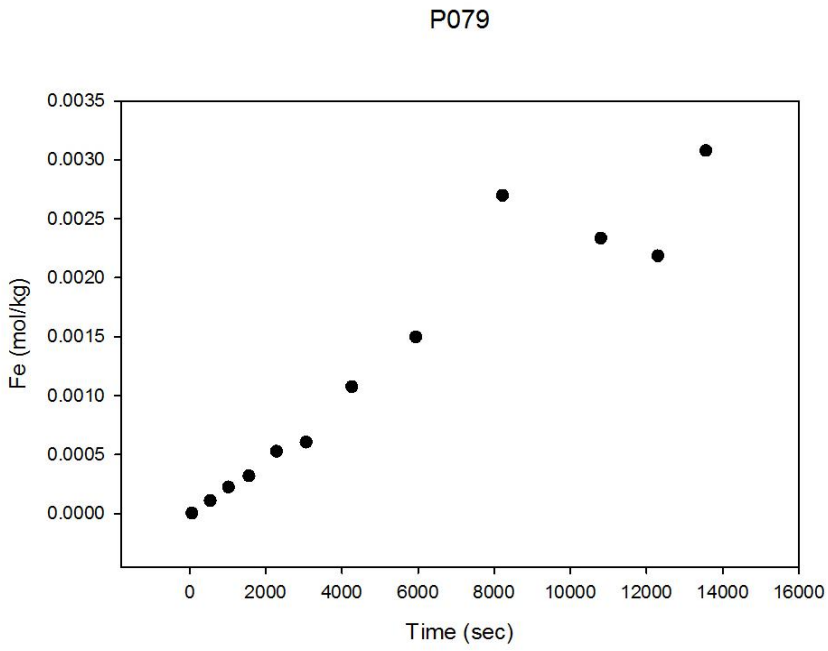

Fig. 24. Duplicate run of P078

It is unclear why runs conducted at pH 7.5 did not accumulate dissolved Fe in the effluent. Additional experiments are necessary to pursue this question. Inconsistencies in Fe data from the two runs conducted at pH 3.0 are would likely be removed with repetition and improvements on the experimental setup.